Tetramethylheptalenes and Their Tricarbonylchromium Complexes: Synthesis, Structures, and Thermal Rearrangements

by **Peter Uebelhart**, **Anthony Linden**, and **Hans-Jürgen Hansen***

Organisch-chemisches Institut der Universität Zürich, Winterthurerstrasse 190, CH-8057 Zürich

and **Yuri A. Ustynyuk***, **Olga A. Trifonova**, **Novruz G. Akhmedov**, and **Vadim I. Mstislavsky**

Department of Chemistry, M.V. Lomonosov Moscow State University, Leninskie Gory, 119888 Moscow, Russian Federation

The thermal 4:1 equilibrium mixture of 1,3,5,6- and 1,3,5,10-tetramethylheptalene (**13a** and **13b**, resp.) has been prepared, starting from the thermal equilibrium mixture of dimethyl 6,8,10-trimethylheptalene-1,2- and -4,5-dicarboxylate (**6a** and **6b**, resp.; *cf. Scheme 5*). These heptalenes undergo double-bond shifts (DBS) even at ambient temperature. Treatment of the mixture **13a**/**13b** 4:1 with $[Cr(CO)_3(NH_3)_3]$ in boiling 1,2-dimethoxyethane resulted in the formation of all four possible mononuclear $Cr(CO)_3$ complexes **19a**–**19d** of **13a** and **13b**, as well as two binuclear $Cr(CO)_3$ complexes **20a** and **20b**, respectively, in a total yield of 87% (*cf. Scheme 7*). The mixture of complexes was separated by column chromatography, followed by preparative HPLC (*cf. Fig. 2*). The structures of all complexes were established by X-ray crystal-structure analyses (complex **19b** and **20b**; *cf. Figs. 6–8*) and extensive ^{1}H-NMR measurements (*cf. Table 3*). In **20b**, the two $Cr(CO)_3$ groups are linked in a '*syn*'-mode to the highly twisted heptalene π-skeleton. The correspondence of the ^{1}H-NMR data of **20a** with that of **20b** indicates that the two $Cr(CO)_3$ groups in **20a** also have a '*syn*'-arrangement. The thermal behavior of the mononuclear complexes **19a**–**19d** has been studied at 85° in hexafluorobenzene (HFB). At this temperature, all four complexes undergo rearrangement to the same thermal equilibrium mixture (*cf. Table 8*). The rates for the thermal equilibration of each complex have been determined by ^{1}H-NMR measurements (*cf. Figs. 9–12*) and analyzed by seven different kinetic schemes (*Chapt. 2*). The equilibration rates are in agreement with two different haptotropic rearrangements that take place, namely intra- and inter-ring shifts of the $Cr(CO)_3$ group, whereby both rearrangements are accompanied by DBS of the heptalene π-skeleton (*cf. Scheme 9*). All individual kinetic steps possess similar $\Delta G^{\neq}$ values in the range of 29–31 kcal·mol^{-1} (*cf. Table 8*). The occurrence of inter-ring haptotropic migrations of $Cr(CO)_3$ groups has already been established for anellated aromatic systems (*cf. Scheme 10*); however, it is the first time that these rearrangements have been unequivocally demonstrated for $Cr(CO)_3$ complexes of non-planar bicyclic [4*n*]annulenes, such as heptalenes. The mechanism of migration may be similar to that proposed for aromatic systems (*cf. Schemes 10* and *11*).

1. Introduction. – The chemistry of heptalenes, which are non-planar bicyclic 12π-electron systems, has been a fast-developing field of research during the last twenty years [1–4]. Numerous X-ray crystal-structure analyses of substituted heptalenes (see references in *Table 1*) have shown that both seven-membered rings adopt boat-like conformations (*Fig. 1*). Thus, the heptalene skeleton can be considered to be a combination of two cycloheptatriene substructures anellated along the C(5a)–C(10a) bond, which, overall, forms two intercalated heptafulvenes.

There is an obvious alternation of C=C and C–C bonds in the molecules. For the structures listed in *Table 1*, the average interatomic distances are 1.350(10) Å for C=C

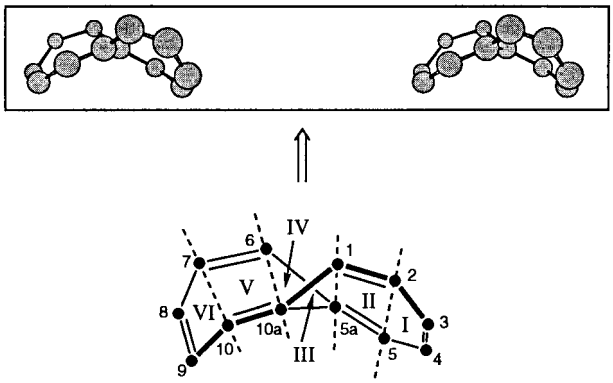

Fig. 1. *Heptalene planes according to* Table 1 *and in relation to the carbon backbone of* **13a** *as a stereoview* (AM1 calculation)

and 1.463(20) Å for C–C bonds. The central C(5a)–C(10a) bond is always the longest C–C bond in heptalenes (average interatomic distance 1.479(8) Å). The magnitudes of the torsion angles in heptalenes and the angles between the planes I, II, III, IV (see *Fig. 1*) are mainly determined by the number, nature, and position of the substituents in both halves of the molecules. The geometry of unsubstituted heptalene has not been studied experimentally, but advanced *ab initio* and DFT quantum-chemical calculations on MP2/6-31G* and BP86/6-31G* levels are available and can be taken into account for qualitative evaluations [5]. There is a pronounced double-bond conjugation within each seven-membered ring (see also [4]). The '*cisoid*' (C=C–C=C) torsion angles of the heptalene perimeter are 27° for heptalene itself (MP2/6-31G*), and vary in the range 27–39° for substituted heptalenes (from crystallographic data) with a mean value of 33(2)°. At the same time, the efficiency of conjugation between both seven-membered rings is rather low, because the '*transoid*' inter-ring (C=C–C=C) torsion angles are much smaller than 180°. This torsion angle is 126.5° for heptalene itself (MP2/6-31G*), and varies from 111 to 123° for substituted heptalenes (mean value 115(3)°; see planes III/IV in *Table 1*). The angles between the planes I/II, II/III, and III/IV, which characterize the planarity of the heptalene core, are very sensitive to the substitution pattern. A number of representative examples from the literature are compiled in *Table 1*. Substituents in the *peri*-positions 1, 5, 6, and 10 play a crucial role. Even just one substituent in one of these positions causes extraordinary changes, and the discussed dihedral angles increase substantially. In heptalenes with three or four *peri*-substituents, the inter-plane angles vary only in the small range of ±3°.

In a manner similar to 8π- and other 12π-annulenes, heptalenes undergo π-skeletal rearrangements which consist of cyclic double-bond shifts (DBS) through non-planar transition states, in which the relevant heptalene core has D_2 symmetry. Other symmetries can be ruled out experimentally [2][16]. The barriers of activation, which separate the twisted double-boat conformations of the DBS isomers of heptalenes, are mainly dependent on the number and bulkiness of the *peri*-substituents [2][16]. For heptalene itself, the barrier of activation for the DBS process is as small as 3.5 kcal/mol

Table 1. *Dihedral Angles in Heptalenes* [°] (E = MeOCO)

Entry	Substituents	Plane I/II[a])	Plane II/III	Plane III/IV	Plane IV/V	Plane V/VI	Plane II/V	Ref.
1	None	21.6	43.9	56.5	43.9	21.6	47.9	[b])
2	None	14.0	29.8	40.6	29.8	14.0	31.3	[c])
3	3,8-E	14.9	29.9	39.3	29.9	14.9	34.0	[6]
4	1,2-E	27.7	42.0	59.5	43.0	22.3	45.4	[7][d])
5	6-[(*E*,*E*)-Ph(CH=CH)$_2$], 4,5-E, 9-Me	26.0(1)	44.8(2)	62.5(2)	50.4(2)	25.0(2)	52.2(1)	[8]
6	1-[(*E*,*E*)-Ph(CH=CH)$_2$], 4,5-E, 6,8,10-Me	26.7(2)	52.6(2)	67.8(2)	52.7(2)	28.0(1)	58.6(1)	[9]
7	1-[(*E*,*E*)-Ph(CH=CH)$_2$], 4,5-E, 6-Me, 9-(i-Pr)	23.9(2)	51.8(3)	67.5(3)	51.0(3)	26.0(2)	56.6(2)	[9]
8	1,3,5,6,8,10-Me	25.7(1)	51.0(2)	63.0(2)	52.5(2)	28.5(1)	58.5(1)	[7][10]
9	1-[(*E*)-Ph(CH=CH)], 2-E, 5,10-Me, 7-i-Pr	29.8(1)	54.2(2)	66.7(29	46.4(2)	26.3(1)	55.1(19)	[11]
10	1,2,6,8,10-Me, 4,5-E	29.6(1)	53.2(2)	67.9(2)	53.2(2)	27.6(1)	58.8(1)	[12]
11	1-(4-MeO−C$_6$H$_4$), 4,5-E, 6,8,10-Me	26.0(1)	52.4(1)	69.1(2)	54.5(1)	29.0(1)	59.8(1)	[4]
12	2-[(*E*)-Ph(CH=CH)], 4,5-E, 6,8,10-Me	31.1(2)	46.5(3)	63.9(3)	48.6(2)	25.1(2)	52.2(2)	[4]
13	1-[(*E*)-Ph(CH=CH)], 4,5-E, 6,8,10-Me	26.4(1)	52.5(2)	68.1(2)	53.9(2)	28.5(1)	59.6(1)	[4]
14	2-Ph, 4,5-E, 6,8,10-Me	29.4(1)	48.7(1)	65.7(2)	51.4(1)	28.0(1)	54.6(1)	[4]
15	1-Me, 4,5-E, 9-(i-Pr), 6-[(*E*)-Ph(CH=CH)]	26.0(1)	49.9(2)	66.2(2)	52.0(2)	25.8(1)	56.0(1)	[4]
16	1,8,10-Me, 3,4-E	30.1(2)	46.8(2)	60.6(3)	48.5(2)	23.9(2)	52.6(2)	[13]
17	1,2-E, 3,4,5,6,8,10-Me	31.3(3)	51.1(4)	63.5(4)	51.5(4)	28.0(3)	57.1(2)	[12]
18	1,2-E, 3,5,6,10-Me, 8-Pr	29.4(4)	53.4(5)	62.8(6)	50.8(5)	26.4(4)	58.4(3)	[12]
19	1,6,8,10-Me, 4,5-E; mol. A	28.3(2)	53.4(3)	69.0(4)	52.9(3)	27.1(2)	59.3(2)	[2][14]
	mol. B	28.1(2)	51.8(3)	63.8(4)	53.5(3)	27.9(2)	59.6(2)	
20	1,3-E, 5,10-Me, 7-(i-Pr)	27.1(2)	50.1(3)	56.8(4)	47.8(3)	26.1(2)	56.2(2)	[15]
21	1,6-Me, 4,5-E, 9-(i-Pr)	27.3(2)	50.2(3)	67.3(3)	51.2(3)	26.6(2)	55.5(2)	[15]
22	1,6,10-Me, 4,5-E, 8-(*t*-Bu)	26.4(2)	52.0(2)	68.3(3)	52.0(2)	28.2(2)	57.6(2)	[16]
23	1,2-E, 5,6,10-Me, 8-(*t*-Bu)	28.5(1)	52.1(2)	66.2(2)	52.0(2)	29.0(1)	58.0(1)	[16]

[a]) Planes I, II, and III always involve the ring with the ester substituents, when present (E = MeOCO). [b]) MP2/6-31G* data [5]. [c]) BP86/6-31G* data [5]. [d]) Recalculated from the atomic coordinates in [7].

[17][1]). It increases to 9.9 kcal/mol for heptalene-1,6-dicarbaldehyde [20], to 14.0 kcal/mol for dimethyl heptalene-1,6-dicarboxylate [20], and to 26.7 kcal/mol for 1,2,5,6,8,10-hexamethylheptalene [2][21]. Several *peri*-substituted heptalenes were isolated as individual DBS isomers, and their optical isomers were also resolved [2][4][22].

Much less data are available about organometallic derivatives of heptalenes. The very first compound of this family, tricarbonyl(η^6-heptalene)chromium (**1**), has been synthesized by *Vogel et al.* [17]. According to its NMR spectra, a rapid 1,2-shift of the Cr(CO)$_3$ group with concomitant DBS occurs in this molecule, even at ambient temperature, so that the molecule acquires on 'effective' mirror plane passing through C(3), C(8), and the central σ-bond (*Scheme 1*). The mono- and binuclear tricarbonyliron complexes **2** and **3** with η^4-coordination of the Fe(CO)$_3$ groups have also been

[1]) In contrast to cyclooctatetraenes as representatives of non-planar 8π-systems (*cf.* [18] and literature cited therein), the racemization process of *peri*-substituted heptalenes, which, in general, can be regarded as ring inversion of both seven-membered rings (double-ring inversion process), always possesses a higher activation barrier than the DBS process [14][16]. Molecular-modeling calculations indicate that the racemization of heptalenes [2], as well as of double-bond-fixed benzo[*a*]heptalenes (*cf.* [3][19]), also takes place *via* non-planar transition states. The measured value of 3.5 kcal/mol for heptalene itself has, therefore, to be regarded as an upper value for the DBS process. Moreover, calculations show that in this case the double ring inversion results in a planarization of the whole molecule [2].

prepared and investigated by X-ray crystal-structure analyses and dynamic NMR spectroscopy [20][23][24]. Intramolecular intra-ring 1,2-migration of the $Fe(CO)_3$ group in **2** has been found (D-NMR data) to proceed rapidly at ambient temperature (*Scheme 2*).

Scheme 1

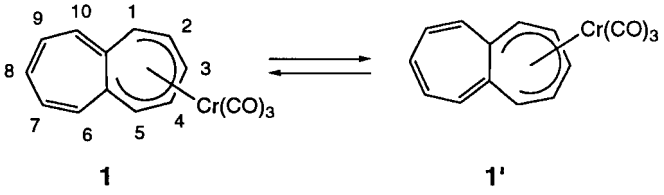

Scheme 2

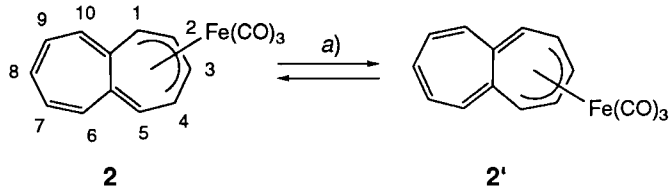

[a]) $\Delta G^{\#}_{273} = (11.4 \pm 1.0)$ kcal/mol, $\Delta H^{\#}_{273} = 10.3$ kcal/mol, $\Delta S^{\#}_{273} = (-4.2 \pm 0.6)$ e. u.

The two $Fe(CO)_3$ groups in **3** are attached to the same face of the ligand (*cis*-configuration; *Scheme 3*). Recently, it has been found by *Lindner* and co-workers that treatment of 1,6-dimethylheptalene with $Fe_2(CO)_9$ in acetone at ambient temperature results in the formation of the corresponding $Fe(CO)_3$ complex, accompanied by the *cis*- and *trans*-configured binuclear complexes, the latter in excess [25]. The structures of both binuclear $Fe(CO)_3$ complexes were determined by X-ray crystal-structure analysis. The activation parameters for the 1,2-shifts of both $Fe(CO)_3$ groups in **3** were found to be higher than those for the 1,2-process in **2** [24]. It was not established whether the shift of the two $Fe(CO)_3$ groups takes places simultaneously or sequentially.

Scheme 3

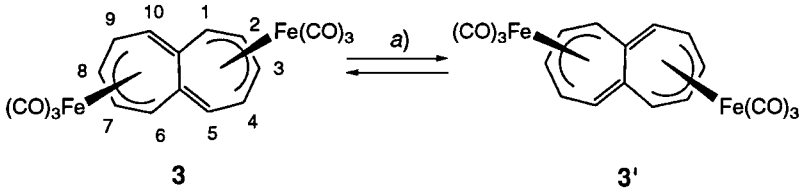

[a]) $\Delta G^{\#}_{273} = (19.8 \pm 0.1)$ kcal/mol, $\Delta H^{\#}_{273} = (24.0 \pm 0.6)$ kcal/mol, $\Delta S^{\#}_{273} = (15.1 \pm 1.6)$ e. u.

Four isomeric $Cr(CO)_3$ complexes **5a**–**5d** of 1,2,5,6,8,10-hexamethylheptalene (**4a**) and its DBS isomer **4b** (see *Scheme 4*), as well as two isomeric binuclear complexes, have been prepared by us previously, and the structure of **5c** has been determined by X-ray crystal-structure analysis [26]. A preliminary study has also shown that, beside decomplexation, two thermally inducible rearrangements proceed in **5c**: *i*) intra-ring

1,2-shift of the $Cr(CO)_3$ group which leads to **5d**, and *ii*) inter-ring migration of the $Cr(CO)_3$ group, which yields **5b** (*Scheme 4*). Both processes are much slower than the 1,2-shift of the $Fe(CO)_3$ groups in **2** and **3**. Due to the concomitant thermal decomplexation reaction of **5c**, it was not possible to conclude from our data whether the formation of **5d** and **5b** took place intra- and/or intermolecularly.

Scheme 4

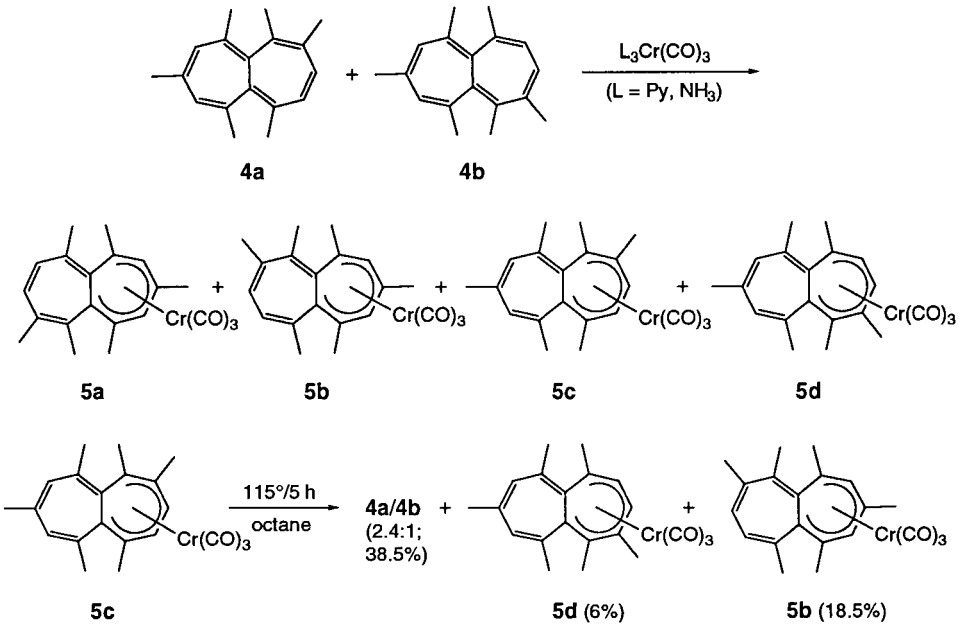

Complexation of organic π-ligands by (transition-metal) carbonyl groups changes the reactivity of the ligands profoundly and is, therefore, often applied in 'transition-metal-mediated' organic synthesis [27]. To obtain more information on the structure and reactivity of $Cr(CO)_3$ complexes of heptalenes, we prepared several new complexes of polysubstituted heptalenes and studied their thermal rearrangements in more detail.

2. Results and Discussion. – 2.1. *Synthesis of Starting Heptalenes.* Since our earlier experiments had indicated that $Cr(CO)_3$ complexes of heptalenes may also undergo thermal inter-ring migration of the $Cr(CO)_3$ group, in addition to thermal intra-ring 1,2-switches (see *Scheme 4*), we were interested in a more detailed study of the dynamic behavior of $Cr(CO)_3$ complexes of such non-planar bicyclic π-systems. However, our preliminary results with complex **5c** had also revealed the fact that the occupancy of all four *peri*-positions in these complexes by Me groups leads to activation barriers close to those for the decomplexation reactions (see *Scheme 4*). Therefore, we decided to synthesize methylated heptalenes with only three substituents in *peri*-positions, since heptalenes of this type exhibit, as a rule, rapid DBS even at room temperature (*cf.* [4]).

Several years ago, *Hafner et al.* [28] reported on the synthesis of Me-substituted heptalenes from dimethyl heptalene-1,2- and -4,5-dicarboxylates, which were reduced to the corresponding heptalene-dimethanols (see *Scheme 5*). The latter compounds underwent acid-induced disproportionation reactions to heptalene-carbaldehydes on heating in benzene in the presence of catalytic amounts of TsOH. The carbaldehydes were then decarbonylated with equimolar amounts of *Wilkinson*'s catalyst ($[Rh^{I}(Ph_3P)_3Cl]$) to give Me-substituted heptalenes. We followed this synthetic scheme by starting from 4,6,8-trimethylazulene and dimethyl acetylenedicarboxylate (ADM; *Scheme 5*), and slightly modified the reaction conditions according to our own experiences with this type of reaction. The thermal reaction leading to the equilibrium mixture of **6a** and **6b** proceeds much more smoothly in MeCN at 100° than in tetralin at 207° [2]. The by-product **7** is formed in only trace amounts in MeCN at 100° ([28]: 8%). The reduction of the mixture **6a**/**6b** with DIBAH in THF at 0° led to a mixture **8a**/**8b**, from which only **8b** crystallized (see also [28][2]). Heating **8b** in toluene at 80° for 10 min led to a complete conversion of **8b** to the thermal 5.8 : 1 equilibrium mixture **10a**/**10b**[3]). Following our original idea, we reduced **8b** with DIBAH in THF to a thermal 3.3 : 1 equilibrium mixture of the heptalenyl-methanols **11a** and **11b**. However, whereas azulene-2-methanols can easily be reduced to the corresponding 2-methylazulenes with Et_3SiH/CF_3COOH (*cf.* [29]), this procedure failed completely in the case of the mixture **11a**/**11b**. Treatment of **11a**/**11b** with MnO_2 in CH_2Cl_2 led back to the mixture **10a**/**10b**. Because of our unsuccessful attempts to synthesize a mixture of the pentamethylheptalenes **12a and 12b**, which are structurally most closely related to the hexamethylheptalenes **4a** and **4b**, we finally decarbonylated the thermal equilibrium mixture **10a**/**10b** with *Wilkinson*'s catalyst to the thermal 4 : 1 equilibrium mixture of the tetramethylheptalenes **13a** and **13b**[4]). This mixture could not be separated into the two DBS forms on a preparative scale, since the thermal DBS process is already too fast at room temperature.

The synthesis of the heptaleno[1,2-*c*]furan **16**, which we intended to test with regard to its behavior as a possible ligand for the $Cr(CO)_3$ group, was realized according to

---

[2]) Heptalene **8b** is obtained as fine light-yellow crystals from acetone/hexane. In some of our experiments, we observed the formation of these light-yellow crystals in an admixture with orange-colored rhombic crystals. These crystals represented the pure DBS isomer **8a**. However, in two cases the ^{1}H-NMR analysis showed them to consist of 2,10a-dihydro-6*H*-heptaleno[1,10-*bc*]furan-3-methanol **9**, which, on heating in acetone/hexane and subsequent crystallization, is completely reverted to crystals of **8b**.

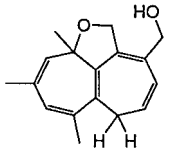

9

[3]) *Hafner et al.* [28] reported the formation of a mixture **10a**/**10b** 20 : 1. However, they crystallized the original mixture of carbaldehydes, which led, *via* the DBS process, to crystals of pure **10b**. Presumably, the ^{1}H-NMR spectrum was recorded before thermal equilibration took place.

[4]) *Hafner et al.* [28] reported the formation of a mixture **13a**/**13b** 3 : 1. AM1 Calculations of both heptalenes lead to a $\Delta\Delta H_f^0 = 0.85$ kcal/mol which should be comparable with $\Delta\Delta G_{298}$, because both compounds will have similar entropies. Indeed, a 0.85 kcal/mol energy difference corresponds to a 81 : 19 mixture **13a**/**13b**, in excellent agreement with the observed 4 : 1 ratio.

Scheme 5

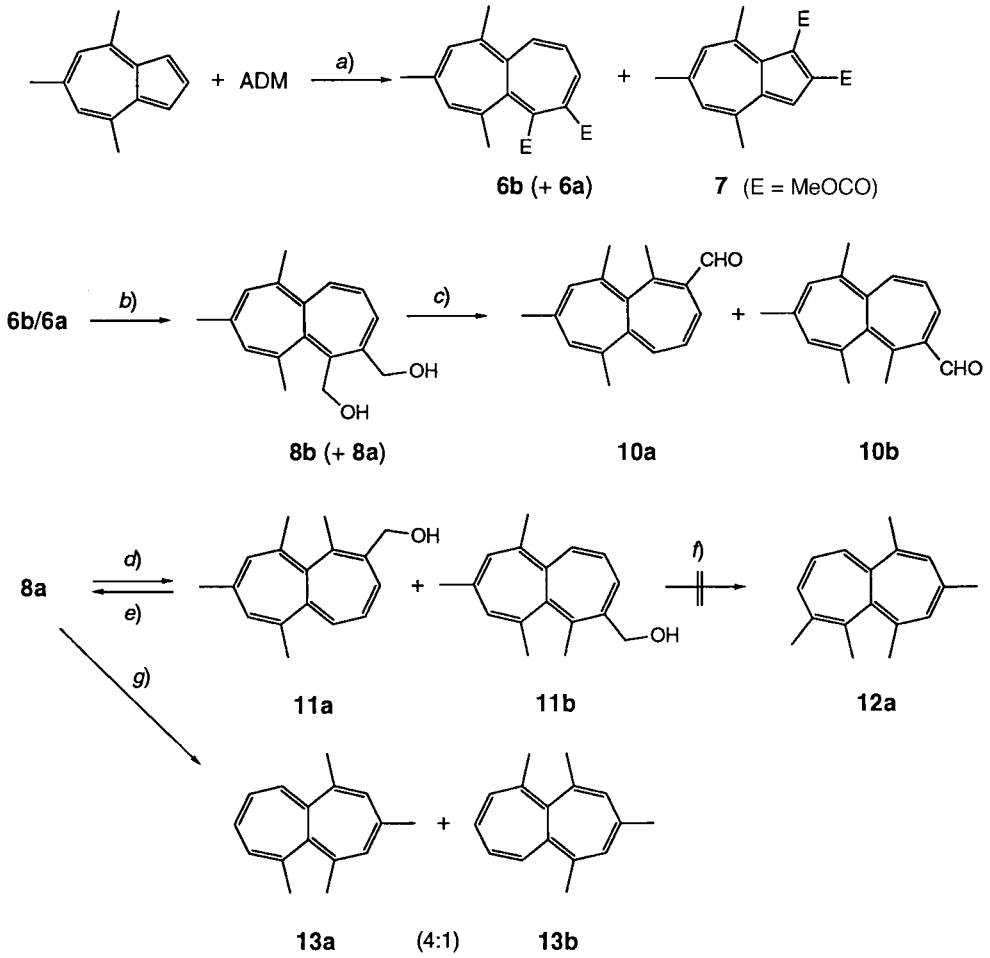

a) 4.5 mol-equiv. ADM in MeCN, 100°, 24 h; 48% of **6a**/**6b**, traces of **7**. *b*) 2M DIBAH in hexane/THF, 15°; 50% of **8a**/**8b**. *c*) Cat. amount of TsOH in toluene, 80°, 10 min; 72% of **10a**/**10b**. *d*) 2M DIBAH in hexane/THF, 0°; 81% of **11a**/**11b**. *e*) MnO_2 in CH_2Cl_2, 20°. *f*) Et_3SiH in TFA, 60°, 4 h; decomposition. *g*) 1. As under *c*, 2. $[Rh(Ph_3P)_3Cl]$ in toluene, 120°, 3 h; 35% of **13a**/**13b**.

procedures developed during our earlier investigations of the formation of this new class of heptaleno compounds (see *Scheme 6*) [30]. Reduction of the heptalene-4,5-dicarboxylate **14b** [12] with DIBAH gave the corresponding heptalene-4,5-dimethanol **15b**, which, on treatment with MnO_2 in CH_2Cl_2, was converted to a mixture of **16**, and the two isomeric heptaleno[1,2-*c*]furanones **17a** and **18a**[5]). This mixture could be easily

[5]) In later experiments we found that the transformation of vicinal heptalene-dimethanols into heptaleno[1,2-*c*]furans can be realized in much better yields and without the occurrence of heptalenofuranones by using 1-hydroxy-1,2-benziodoxol-3(1*H*)-one 1-oxide (IBX [31]) as the oxidizing agent [32].

separated by chromatography on silica gel, finally providing pure **16** as light-yellow crystals after crystallization from hexane. Compounds **17a** and **18a** were also obtained in pure form after crystallization. Their ^{1}H-NMR spectra showed no additional signals that could be attributed to the corresponding DBS forms, **17b** and **18b**, of **17a** and **18a**, respectively.

Scheme 6

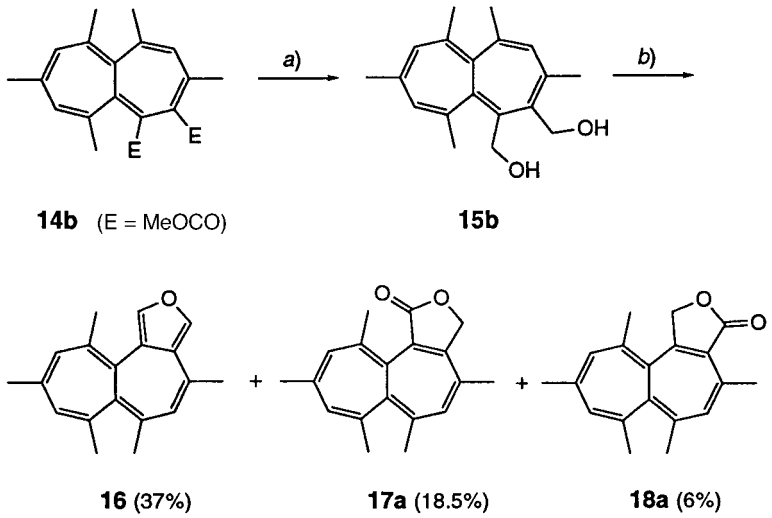

14b (E = MeOCO) **15b**

16 (37%) **17a** (18.5%) **18a** (6%)

a) 2M DIBAH in hexane/THF, 0°; 89% of **15b**. *b*) MnO_2 in CH_2Cl_2, 20°, 40 min; 87%.

2.2. *Formation and HPLC Separation of the Cr(CO)$_3$ Complexes of Heptalenes. Rausch*'s reaction [33] has been employed for the preparation of the $Cr(CO)_3$ complexes. The thermal equilibrium mixture **13a**/**13b** and $[Cr(CO)_3(NH_3)_3]$ was added in equimolar amounts to 1,2-dimethoxyethane (DME). Boiling the reaction mixture for 2 h led to 87% conversion. As we had found previously for the complexation of the hexamethylheptalenes **4a** and **4b** [26], all four possible mono-nuclear complexes, **19a**–**19d**, and two dinuclear complexes, **20a** and **20b**, were formed (*Scheme 7*). The tetramethylheptalenes **13a** and **13b** are more reactive in the *Rausch* reaction than their hexamethyl analogues **4a** and **4b**, and the total yield (83%) of the mononuclear complexes **19a**–**19d** is high. Complexes **19a** and **19d** are thermodynamically more stable than complexes **19b** and **19c**, leading to the predominance of the former complexes in the reaction mixture. We assume that the greater stability of the complexes **19a** and **19d** is due to the coordination of the $Cr(CO)_3$ group with that C-atom (C(1)), which is sterically less encumbered, *i.e.*, there are no opposing Me groups in the adjacent *peri*-positions, in contrast to the situation in the complexes, **19a** and **19d**.

The isolated reaction mixture, containing complexes **19a**–**19d**, as well as the dinuclear complexes **20a** and **20b**, could be separated by HPLC on a *Spherisorb NH$_2$* column with hexane as the eluting solvent (*cf. Fig. 2*), whereby the mononuclear complexes showed base-line separation with the following order of elution: **19b** < **19a** < **19d** < **19c**. Under these conditions, the more polar dinuclear complexes **20a** and

Scheme 7

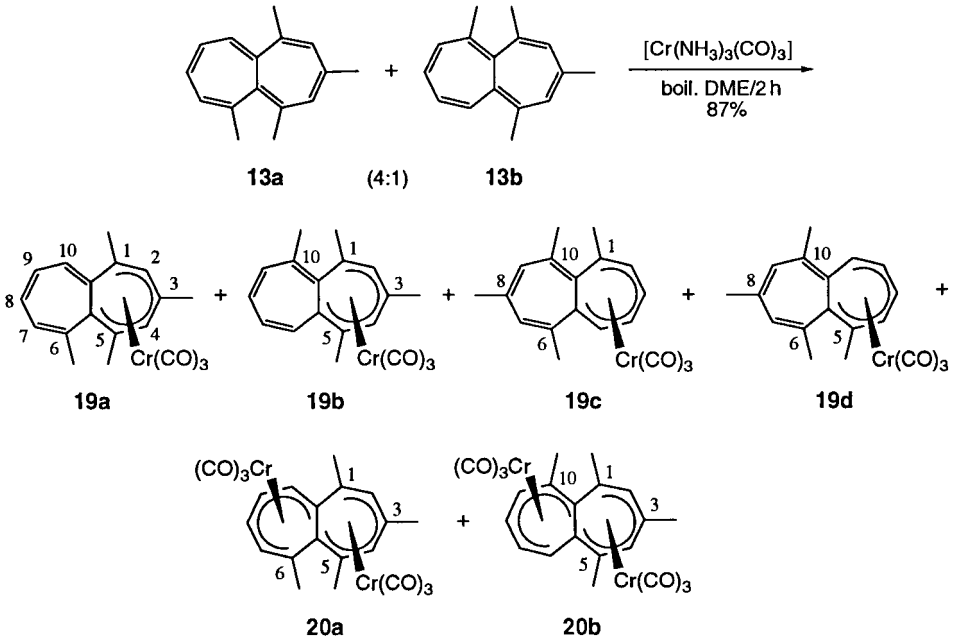

20b were completely retained on the column. However, they could be washed from the column by elution with hexane/CH_2Cl_2 2 : 1. Subsequent chromatography of the mixture **20a**/**20b** on the column with hexane/CH_2Cl_2 3 : 1 then led to a nearly complete separation of **20a** and **20b**. All six complexes could be crystallized from benzene/heptane (**19a** – **19d**) or Et_2O/hexane (**20a** and **20b**), and were obtained as dark-red crystals. The crystals of **19b** and **20b** were suitable for X-ray crystal-structure analyses (see *Sect. 2.3*).

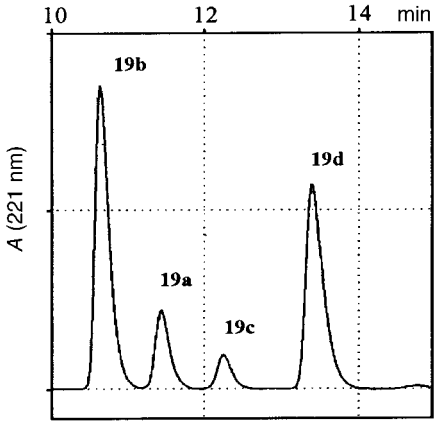

Fig. 2. *HPLC Separation of a mixture of* **19a** – **19d** *on the analytical* Spherisorb NH_2 *column with hexane as the mobile phase* (for details, see *Exper. Part*)

All six complexes show, as expected, very similar UV/VIS spectra with only small variations in their λ_{max} values (*cf. Fig. 3* and *Table 2*). The shapes of the spectra are mainly characterized by the four heptalene absorption bands I to IV (see [4]) of the free ligands **9a** and **9b** (*cf. Fig. 4*), with a clear enhancement of the extinctions of bands I and II in all six complexes. Of the two pairs of DBS isomers, namely **19a**/**19b** and **19c**/**19d**, the complexes with optimal Me substitution of the coordinated heptafulvene substructure, *i.e.*, **19b** and **19c**, exhibit the heptalene band I at longer wavelengths, most probably due to optimal hyperconjugative effects in these complexes.

Table 2. *UV Spectra of the Cr(CO)$_3$ Complexes and Their Corresponding Heptalene Ligands*[a])

Compound	λ_{max} [nm][b])				Solvent
	I	II	IIIa/IIIb	IV	
13a	~400[c])	318	252/240 (sh)	208	Hexane
13b	~400[c])	312	255/243 (sh)	205	Hexane
19a	420 (sh)	360	265 (sh)	222	Hexane
19b	423	344	270 (sh)	220	Hexane
19c	431	342	270 (sh)	221	Hexane
19d	420 (sh)	344	270 (sh)	221	Hexane
20a	430	342sh/311sh	277 (sh)	218	Hexane/7% i-PrOH
20b	420	342sh/311sh	277 (sh)	218	Hexane/7% i-PrOH
16	~400[c])	322	275/237 (sh)	216/210	Hexane

[a]) UV Spectra of **13a**, **13b**, **19a**–**19d**, **20a**, **20b** were recorded with the photo-diode array detector of the *Waters* instrument; for spectra of **19a**–**19d** and **20a** and **20b**, see also *Figs. 3* and *4*. [b]) For band assignments, see [4]. [c]) Estimated λ values according to the observed long tailing.

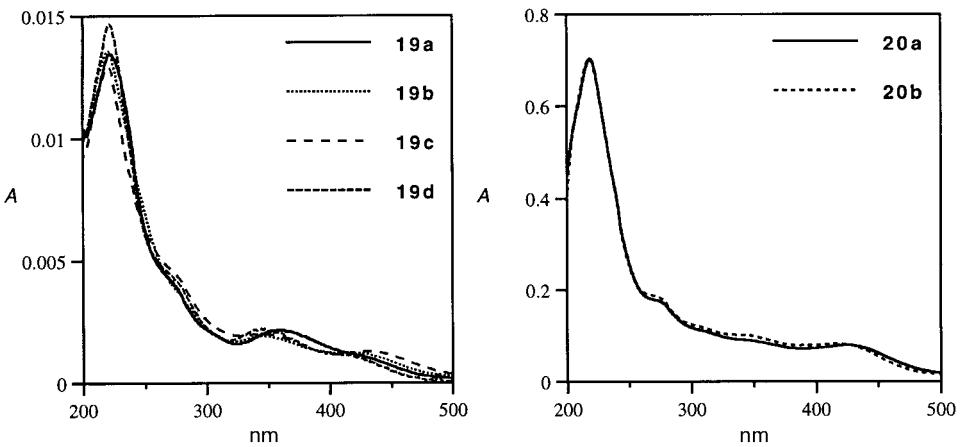

Fig. 3. *UV/VIS Spectra of* **19a**–**19d** *in hexane* (left), *and of* **20a** *and* **20b** *in hexane/7% i-PrOH* (right; *cf. Table 2*)

The ^{1}H-NMR spectra of all six complexes allow an unequivocal assignment of their individual structures (see *Table 3* for chemical shifts and coupling patterns). The two DBS sets of mono-nuclear complexes **19a**/**19b** and **19c**/**19d** can be distinguished by the observed chemical-shift differences of the H-atoms of the coordinated seven-membered rings. On the other hand, the two isomers in each DBS set are clearly

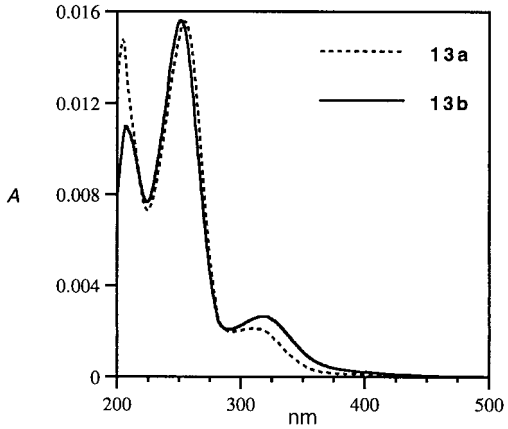

Fig. 4. *UV/VIS Spectra of* **13a** *and* **13b** *in hexane, recorded during HPLC separation with the photo-diode detector of the HPLC system*

characterized by the observed coupling constants, *e.g.*, complex **19a** shows the chemical shift of H–C(10) at 5.01 ppm as a *d* with $^3J(9,10) = 5.9$ Hz, whereas in its DBS form **19b** the analogous H–C(6) appears at 5.48 ppm as a *doublet* with $^3J(6,7) = 10.0$ Hz, confirming that, in complex **19a**, C(9) and C(10) are linked by a single bond, and the analogous C(6) and C(7) in **19b** by a double bond. Similarly, the DBS pair **19c** and **19d** show reduced ^3J(HC=CH) and slightly greater ^3J(CH–CH) values for their coordinated halves, *e.g.*, 7.0 Hz for $^3J(4,5)$ of **19c** and 8.5 Hz for $^3J(1,2)$ of **19d**, indicating a single bond between C(4) and C(5) in **19c**, and a double bond between C(1) and C(2) in **19d**. A comparison of the vicinal coupling constants across C–C bonds of the non-coordinated seven-membered ring in **19a** and **19b** with those of the free ligands reveals that the geometry of the non-coordinated seven-membered rings in the mononuclear complexes must be similar to that of the free ligands. These findings are fully supported by the X-ray crystal-structure analysis of complex **19b** (see next section).

The 600 MHz ^{1}H-NMR spectra of the dinuclear complexes **20a** and **20b** in C_6D_6 are depicted in *Fig. 5*. The assignment of the position of the C=C bonds in these two isomers can be deduced from the observed ^3J values of the *doublet* (integrating for 1 H) that appears in both spectra at highest field. Complex **20a** shows this resonance at 3.31 ppm with $^3J = 7.0$ Hz, while it appears in the spectrum of complex **20b** at 3.10 ppm with $^3J = 8.2$ Hz. The latter signal also exhibits an allylic coupling constant of 0.9 Hz. These observations are compatible only with the shown structures for the two complexes, which are further supported by the magnitudes of the other coupling constants observed in both complexes. In accordance with the given assignments, complex **20a** displays one vicinal coupling constant on the order of 8.2–8.4 Hz and two on the order of 7.0–7.7 Hz, whereas **20b** possesses two on the order of 8.2–8.8 Hz and only one on the order of 6.7–6.8 Hz. However, the ^{1}H-NMR spectra did not allow any conclusion about the relative position of the two $Cr(CO)_3$ groups with respect to each other. The X-ray crystal-structure analysis of complex **20b** confirmed these structural assignments and, furthermore, showed that the two $Cr(CO)_3$

Table 3. *Chemical Shifts* δ [ppm] *and Coupling Constants* J [Hz] *in the* ^{1}*H-NMR Spectra of the Mononuclear* $Cr(CO)_3$ *Complexes* **19a**–**19d** *and the Dinuclear Complexes* **20a** *and* **20b**[a])

Complex[b])	Position of H-atoms or Me groups									
	H/Me–C(1)	H–C(2)	H/Me–C(3)	H–C(4)	H/Me–C(5)	H/Me–C(6)	H–C(7)	H/Me–C(8)	H–C(9)	H/Me–C(10)
19a	1.984	4.091	1.711	5.063	1.650	2.097	5.85–5.70	5.85–5.70	5.85–5.70	5.010
	(br. *s*)	(br. *s*)	(br. *s*)	(*d*, *J* = 0.8)	(*s*)	(*s*)	(*m*)	(*m*)	(*m*)	(*d*, *J* = 5.9)
	2.156	4.66	2.174	5.74	2.02	2.70	6.11	5.98 (br. *dd*,	5.89 (br. *dd*,	5.35
	(*d*, *J* = 0.7)	(br. *s*)	(*d*, *J* = 0.7)	(br. *s*)	(*s*)	(br. *s*)	(br. *d*, *J* = 6.4)	*J* = 11.9, 6.4)	*J* = 11.2, 6.4)	(br. *d*, *J* = 6.4)
19b	1.729	4.427	1.903	5.104	1.800	5.484	5.811 (*ddd*,	5.880 (*ddd*,	5.733	1.179
	(*d*, *J* = 0.7)	(br. *s*)	(*d*, *J* = 0.7)	(br. *s*)	(*s*)	(*d*, *J* = 10.0)	*J* = 10.0, 6.1, 1.2)	*J* = 11.7, 6.3, 0.9)	(*d*, *J* = 11.2)	(*s*)
	2.16	5.03	2.62	5.73	2.10	5.67	6.18	6.18	6.02	1.68
	(*d*, *J* = 0.7)	(br. *s*)	(br. *s*)	(br. *s*)	(*s*)	(*m*)	(*m*)	(*m*)	(*m*)	(*s*)
19c	2.061	4.302	4.997 (*dd*,	4.850 (*ddd*,	3.995	1.599	5.584	1.707	5.525	1.168
	(*d*, *J* = 1.0)	(*d*, *J* = 6.6)	*J* = 8.4, 6.6)	*J* = 8.4, 7.0, 0.7)	(*d*, *J* = 7.0)	(*d*, *J* = 1.3)	(*quint.*-like, 1.2)	(br. *s*)	(br. *s*)	(*s*)
	2.14	5.04	5.86 (*ddd*,	5.73 (*ddd*,	4.48 (*dd*,	2.19	5.91	1.93	5.74	1.65
	(*d*, *J* = 0.7)	(br. *d*, *J* = 6.6)	*J* = 8.4, 6.6, 0.6)	*J* = 8.4, 6.9, 0.8)	*J* = 6.9, 0.6)	(*d*, *J* = 1.0)	(br. *s*)	(*d*, *J* = 1.4)	(br. *s*)	(*s*)
19d	3.190	4.302	5.190 (*ddd*,	4.855	1.217	2.149	5.661	1.641	5.528	1.595
	(*d*, *J* = 8.5)	(*dd*, *J* = 8.5, 6.6)	*J* = 8.8, 6.6, 1.2)	(*d*, *J* = 8.8)	(*s*)	(*d*, *J* = 1.0)	(br. *s*)	(*d*, *J* = 0.8)	(*s*)	(*d*, *J* = 1.0)
	3.81 (*dd*,	5.11 (*ddd*,	6.08 (*ddd*,	5.75	2.04	2.24	6.02	1.95	5.68	1.66
	J = 8.4, 1.1)	*J* = 8.4, 6.6, 0.7)	*J* = 8.8, 6.6, 1.1)	(*dd*, *J* = 8.8, 0.7)	(*s*)	(*d*, *J* = 1.3)	(br. *s*)	(*d*, *J* = 1.3)	(br. *s*)	(*d*, *J* = 0.9)
20a	1.877	4.113	1.893	4.480	1.216	1.930	4.215	4.754 (*ddd*,	4.269 (*ddd*,	3.309
	(*d*, *J* = 0.7)	(br. *s*)	(br. *s*)	(*d*-like, *J* = 1.0)	(*s*)	(*d*, *J* = 0.6)	(*d*, *J* = 7.0)	*J* = 8.2, 7.2, 0.6)	*J* = 8.4, 7.0, 0.7)	(*d*, *J* = 7.0)
20b	1.968	4.376	1.795	4.565	1.255	3.100 (*dd*,	4.297 (*ddd*,	4.853 (*ddd*,	4.248	1.148
	(*d*, *J* = 0.7)	(br. *s*)	(br. *s*)	(br. *s*)	(*s*)	*J* = 8.2, 0.9)	*J* = 8.7, 6.7, 1.1)	*J* = 8.7, 6.7, 1.1)	(*d*, *J* = 8.8)	(*s*)

[a]) Complex **19a**–**19d**, upper entries: δ for C_6D_6 at 300 MHz; lower entries: δ for HFB at 400 MHz. [b]) Complexes **20a** and **20b**: δ for C_6D_6 at 600 MHz; C_6D_5H at 7.160 ppm.

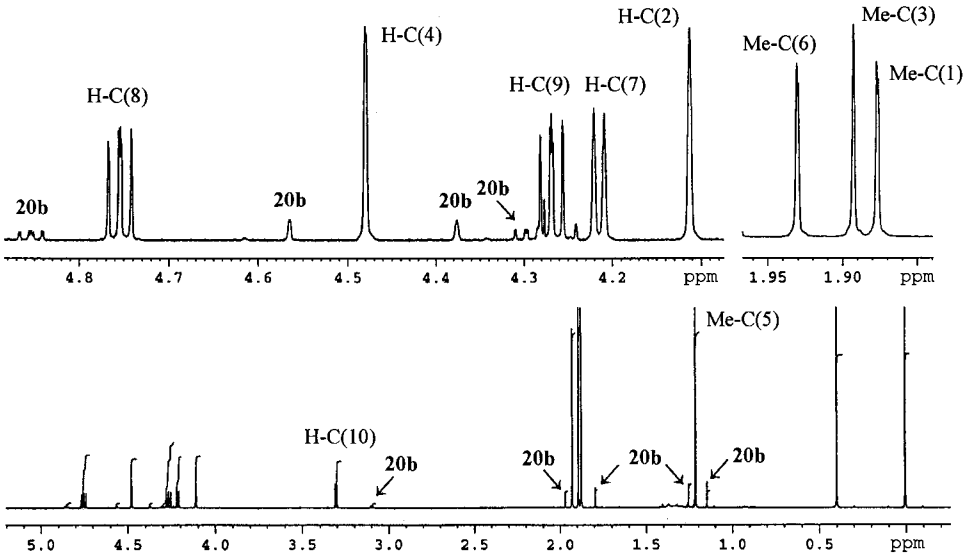

Fig. 5. *^{1}H-NMR Spectrum* (600 MHz; C_6D_6) *of the dinuclear complex* **20a**, *contaminated with* ca. *5% of* **20b**, *after HPLC separation* (*cf. Table 3*)

groups are coordinated to the same face of the heptalene core (see the following section).

Treatment of the heptaleno[1,2-*c*]furan **16** with $[Cr(CO)_3(NH_3)_3]$ under *Rausch*'s conditions led in 60% yield to the corresponding $Cr(CO)_3$ complex **21**, which, after crystallization from hexane, was obtained as dark-red crystals (*Scheme 8*).

Scheme 8

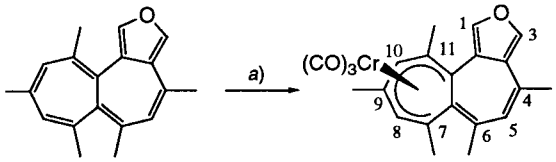

16 **21**

a) $[Cr(CO)_3(NH_3)_3]$ in DME, reflux, 2 h; 63% of **21** with respect to recovered **16** (67%).

2.3. *X-Ray Crystal Structures of Mono- and Dinuclear Chromium Complexes.* Two projections of the mononuclear $Cr(CO)_3$ complex **19b** are shown in *Figs. 6* and *7*. The most important structural parameters are presented in *Tables 4*, *5*, and *6*. The geometry of the complex is generally very close to the geometry of complex **5c**, studied earlier [26]. The presence of the $Cr(CO)_3$ group mainly changes the structural parameters of the seven-membered ring to which it is coordinated. The C=C bond lengths in the coordinated ring of **19b**, with an average of 1.396 Å, differ insignificantly from those in

5c (the average is only 0.006 Å shorter than in **5c**, and, as 0.006 Å is within the error range, we cannot assert that any difference exists), whereas the C–C bond lengths (average value 1.454 Å) are *ca.* 0.026 Å shorter than those in **5c**. The planarization of the coordinated seven-membered ring is similar to that in **5c**. The angle between the planes I/II (defined in *Fig. 1*) is 11.0(2)°, compared with 12° for **5c** and 28(2)°, on average, for free, substituted heptalenes (*cf. Table 1*). Four of the Cr–C bonds, namely those involving C(2) to C(5), have bond lengths of 2.200(3)–2.231(3) Å, which are normal bond lengths for π-coordinated Cr–C bonds. The two Cr–C bonds involving C(1) and C(5a) at the ends of the coordinated π-system are slightly longer (2.368(3) and 2.380(3) Å, resp.). The other central C-atom (C(10a)) is 2.863(3) Å from the Cr-atom and, presumably, does not significantly participate in the coordination. The non-coordinated seven-membered ring changes its geometry little in comparison with the free ligand. The C=C and C–C bonds preserve their usual lengths with average distances of 1.342 and 1.464 Å, respectively. All dihedral angles are within the typical range for heptalenes. Thus, the effects of $Cr(CO)_3$ coordination on the structural parameters of seven-membered rings in heptalenes are similar to those observed for monocyclic $Cr(CO)_3$ complexes, such as tricarbonyl(η^6-tropone)chromium [34]. This similarity provides additional evidence for low inter-ring C=C bond conjugation in heptalenes. The two seven-membered rings in heptalenes are, therefore, quite independent in their behavior with respect to $Cr(CO)_3$ coordination.

Fig. 8 depicts the molecular geometry of the dinuclear complex **20b**. Both Cr-atoms are on the same side of the bicyclic ligand, as found in the dinuclear $Fe(CO)_3$ complex **3**. This mode of coordination is most probably predetermined by the structural features of the mononuclear complexes **19b** or **19d**, which act as starting compounds for the

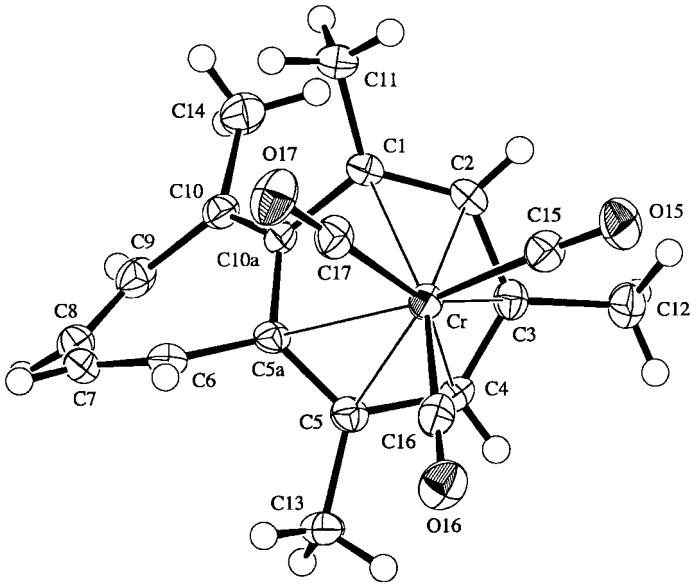

Fig. 6. *ORTEP Representation of the X-ray crystal structure of* **19b** *with atomic numbering* (top-view of the complexed ring)

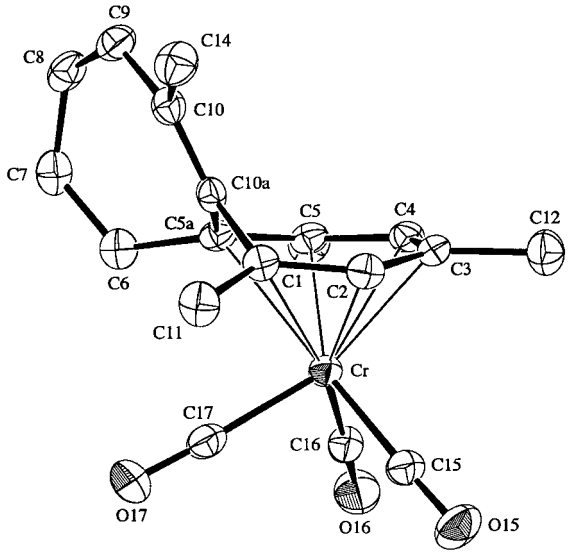

Fig. 7. *ORTEP Representation of the X-ray crystal structure of* **19b** (side-view of the complexed ring; H-atoms are omitted for the sake of clarity)

Table 4. *Selected Bond Lengths for the Mono- and Dinuclear $Cr(CO)_3$ Complexes* **19b** *and* **20b**, *Respectively*

Bond lengths [Å]	**19b**	**20b**
Cr(1)–C(1)	2.369(3)	2.404(5)
Cr(1)–C(2)	2.208(3)	2.217(5)
Cr(1)–C(3)	2.229(3)	2.206(5)
Cr(1)–C(4)	2.200(3)	2.187(6)
Cr(1)–C(5)	2.228(3)	2.223(5)
Cr(1)–C(5a)	2.380(3)	2.296(5)
Cr(1)–C(10a)	2.863(3)	2.832(5)
Cr(2)–C(5a)	–	2.857(5)
Cr(2)–C(6)	–	2.357(5)
Cr(2)–C(7)	–	2.204(6)
Cr(2)–C(8)	–	2.180(6)
Cr(2)–C(9)	–	2.198(6)
Cr(2)–C(10)	–	2.254(6)
Cr(2)–C(10a)	–	2.393(5)
C(1)–C(2)	1.387(4)	1.386(7)
C(1)–C(10a)	1.488(4)	1.503(7)
C(2)–C(3)	1.440(4)	1.428(7)
C(3)–C(4)	1.405(4)	1.390(7)
C(4)–C(5)	1.435(4)	1.438(7)
C(5)–C(5a)	1.396(4)	1.391(7)
C(5a)–C(6)	1.486(4)	1.501(7)
C(5a)–C(10a)	1.481(4)	1.491(6)
C(6)–C(7)	1.338(4)	1.369(7)
C(7)–C(8)	1.447(4)	1.430(8)
C(8)–C(9)	1.341(4)	1.396(7)
C(9)–C(10)	1.460(4)	1.425(7)
C(10)–C(10a)	1.348(4)	1.387(7)

Table 5. *Selected Bond Angles for the Mono- and Dinuclear $Cr(CO)_3$ Complexes* **19b** *and* **20b**, *Respectively*

Bond angles [°]	**19b**	**20b**
C(2)–C(1)–C(10a)	119.3(2)	117.7(5)
C(1)–C(2)–C(3)	127.7(2)	130.3(5)
C(2)–C(3)–C(4)	125.7(3)	126.4(5)
C(3)–C(4)–C(5)	130.3(3)	130.1(5)
C(4)–C(5)–C(5a)	124.3(3)	123.6(5)
C(5)–C(5a)–C(6)	121.6(2)	122.8(5)
C(5)–C(5a)–C(10a)	121.2(3)	121.3(5)
C(6)–C(5a)–C(10a)	115.5(2)	112.0(4)
C(5a)–C(6)–C(7)	122.1(3)	118.5(5)
C(6)–C(7)–C(8)	125.9(3)	126.4(5)
C(7)–C(8)–C(9)	127.1(3)	129.2(5)
C(8)–C(9)–C(10)	128.1(3)	128.7(5)
C(9)–C(10)–C(10a)	123.2(3)	124.5(5)
C(1)–C(10a)–C(5a)	111.5(2)	111.7(4)
C(1)–C(10a)–C(10)	124.3(3)	124.1(5)
C(5a)–C(10a)–C(10)	124.2(2)	121.3(5)

Table 6. *Selected Torsion Angles for the Mono- and Dinuclear $Cr(CO)_3$ Complexes* **19b** *and* **20b**, *Respectively*

Torsion angles [°]	**19b**	**20b**
C(1)–C(2)–C(3)–C(4)	– 13.5(5)	– 10.2(9)
C(1)–C(10a)–C(5a)–C(5)	– 71.0(3)	– 74.2(7)
C(1)–C(10a)–C(5a)–C(6)	123.5(2)	127.6(5)
C(1)–C(10a)–C(10)–C(9)	– 177.2(3)	– 177.8(5)
C(2)–C(1)–C(10a)–C(5a)	71.2(3)	67.3(6)
C(2)–C(1)–C(10a)–C(10)	– 107.2(3)	– 93.5(7)
C(2)–C(3)–C(4)–C(5)	0.9(5)	– 1.1(9)
C(3)–C(2)–C(1)–C(10a)	– 23.1(5)	– 21.7(8)
C(3)–C(4)–C(5)–C(5a)	12.7(5)	7.8(9)
C(4)–C(5)–C(5a)–C(6)	– 172.9(3)	– 174.1(5)
C(4)–C(5)–C(5a)–C(10a)	22.5(4)	30.1(8)
C(5)–C(5a)–C(6)–C(7)	– 107.7(3)	– 86.2(7)
C(5)–C(5a)–C(10a)–C(10)	107.4(3)	87.2(7)
C(5a)–C(6)–C(7)–C(8)	– 4.2(5)	– 25.3(9)
C(5a)–C(10a)–C(10)–C(9)	4.6(4)	23.1(9)
C(6)–C(5a)–C(10a)–C(10)	– 58.1(4)	– 71.0(7)
C(6)–C(7)–C(8)–C(9)	– 29.5(5)	– 12(1)
C(7)–C(6)–C(5a)–C(10a)	57.7(4)	71.6(7)
C(7)–C(8)–C(9)–C(10)	0.3(5)	1(1)
C(8)–C(9)–C(10)–C(10a)	28.6(5)	11(1)

formation of **20b**. The *cis*-face of complex **19b**, as well as that of complex **19d**, is much more accessible for the attack of 'hot' $Cr(CO)_3L_n$ ($n = 0, 1, 2$) particles, generated from $[Cr(CO)_3(NH_3)_3]$ under the conditions of the *Rausch* reaction. The second seven-membered ring in **19b** or **19d** now enters into coordination with a second $Cr(CO)_3$ group. It causes the same changes in geometry as described above for the coordinated seven-membered ring in **19b**. Both rings in **20b** are now more planar (the angles between planes I/II in each ring are 7.3(4)° and 9.5(4)°, resp.; *cf. Tables 4–6*). Substantial elongation of the C=C bonds is observed, as well as a slight shortening of

the C–C bonds. The average bond length is 1.387 Å for the C=C and 1.454 Å for the C–C bonds. The modes of coordination of both $Cr(CO)_3$ groups are similar: four short and two longer Cr–C bonds. As one can see from the data presented in *Tables 4–6*, the coordination of the second $Cr(CO)_3$ group has only a very small influence on the structural parameters of the initially coordinated ring. It is noteworthy that in **20b** the angle between planes II and V (see *Table 7*) is by 13.8° larger than in **19b**. This undoubtedly leads to an additional decrease of the conjugation between the two seven-membered rings. In conclusion, it is apparent that both seven-membered rings in **20b** are independent in their coordination with the $Cr(CO)_3$ groups.

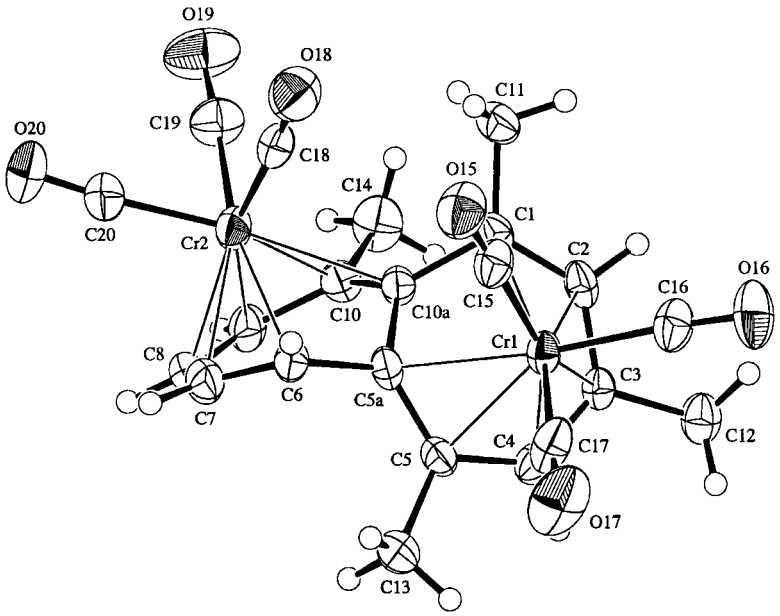

Fig. 8. *ORTEP Representation of the X-ray crystal structure of* **20b** *with atomic numbering*

Table 7. *Dihedral Angles* [°] *in the Complexes* **19b** *and* **20b**[a])

Complex	Substituents	Plane I/II	Plane II/III	Plane III/IV	Plane IV/V	Plane V/VI	Plane II/V
19b	1,3,5,6-Me	11.0(2)	57.8(2)	56.5(3)	46.7(3)	24.2(2)	62.9(2)
20b	1,3,5,10-Me	7.3(4)	58.0(5)	52.5(7)	58.2(6)	9.5(4)	76.7(4)

[a]) For definition of planes, see *Table 1* and *Fig. 1*.

2.4. *Kinetics of the Haptotropic Rearrangements of the Four $Cr(CO)_3$ Complexes.* As discussed above, the thermal conversion of the $Cr(CO)_3$ complex **5c** to **5b** (*Scheme 4*) was the first example of an inter-ring haptotropic rearrangement in non-planar complexes of bicyclic π-systems. We have found, during investigations of the inter-ring haptotropic rearrangement of $Cr(CO)_3$ complexes of planar polycyclic aromatic

ligands, that hexafluorobenzene (HFB) is a very suitable solvent for kinetic measurements of such complexes [35], since HFB does not induce intermolecular ligand-exchange reactions, as has been observed with benzene and other aromatic solvents. The solubility of complexes **19a**–**19d** in HFB is sufficiently high to follow thermal isomerizations by ^{1}H-NMR spectroscopy applying the standard protocol that has been developed for inter-ring haptotropic rearrangements of $Cr(CO)_3$ complexes of substituted naphthalenes [36]. The isomerization kinetics have been studied for all four complexes **19a**–**19d**, starting with the pure forms, at 85° in sealed and degassed NMR tubes. The isomerizations took place smoothly, no other compounds were detected, and, after 200 h, all four complexes showed the same equilibrium composition. The reproducibility of the results has been tested in separate experiments with complexes **19b** and **19c**. The individual kinetic curves are depicted in *Figs. 9–12*.

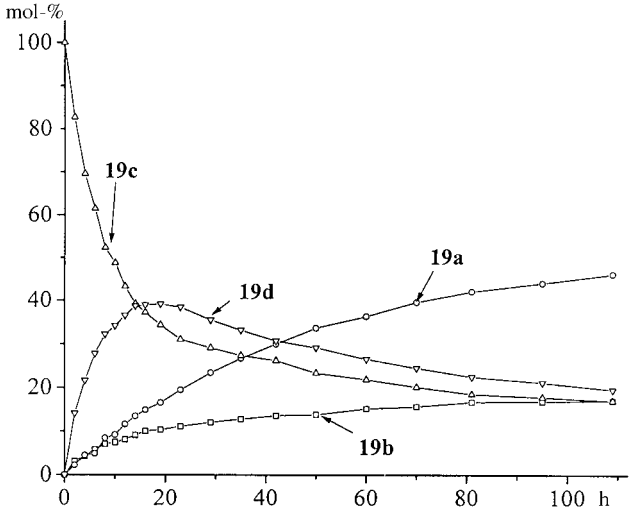

Fig. 9. *Kinetic curves of the thermal isomerization of the pure complex* **19c** (HFB, 85°)

The complete set of kinetic data was processed simultaneously using the software KINETICS-2 (a version of KINETICS), especially designed to analyze complex kinetic schemes, including several parallel and consecutive processes [37]. Seven different kinetic schemes have been tested. The best agreement between the experimental and calculated curves has been obtained for the cyclic processes depicted in *Scheme 9*, which excludes the direct transformations **19b** $\rightleftharpoons$ **19d** as well as **19a** $\rightleftharpoons$ **19c**. The absence of these reaction channels can be recognized qualitatively from the appearence of maxima in the kinetic curves for complexes **19c** and **19d**. All kinetic data are summarized in *Table 8*.

The following conclusions can be drawn from our experiments: *1*) The thermodynamically most stable complex **19a** carries the coordinating $Cr(CO)_3$ group at the seven-membered ring which is substituted with three electron-donating Me groups. This is in good agreement with the substituent effects observed for other polycyclic π-ligands in tricarbonyl chromium complexes. *2*) The 1,2-haptotropic shifts and the inter-

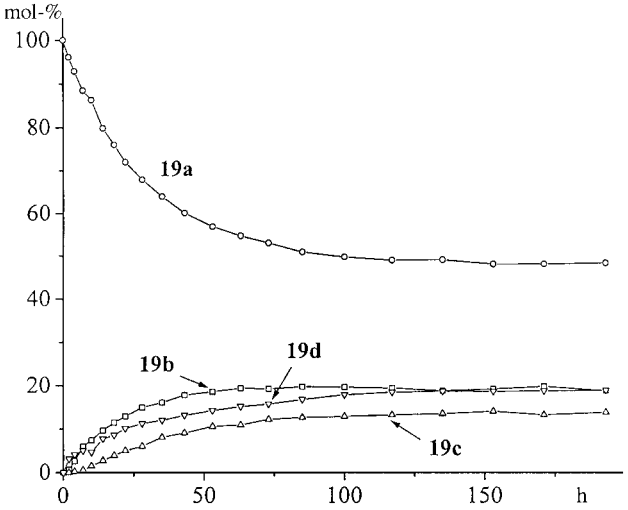

Fig. 10. *Kinetic curves of the thermal isomerization of the pure complex* **19a** (HFB, 85°)

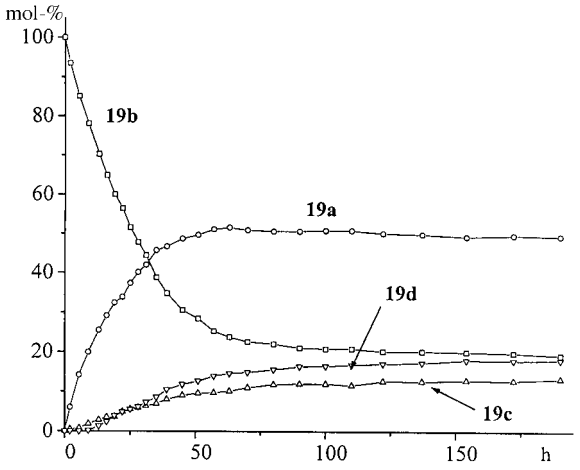

Fig. 11. *Kinetic curves of the thermal isomerization of the pure complex* **19b** (HFB, 85°)

ring haptotropic migrations of the $Cr(CO)_3$ group proceed as intramolecular processes. *3*) The activation barriers for both processes are quite similar. *4*) The free energies of activation for the inter-ring haptotropic rearrangement in complexes **19a**–**19d** do not differ significantly from those for η^6,η^6-inter-ring haptotropic rearrangements of planar $Cr(CO)_3$ complexes of substituted naphthalenes, which were determined under the same conditions.

The inter-ring migration of the $Cr(CO)_3$ group in complexes with polycyclic aromatic and hydroaromatic ligands proceeds through transition states for η^4-trimethylene methane-type structures in which the metal is coordinated to four C-atoms [38]. For example, the transition state has C_{2v} symmetry for the inter-ring

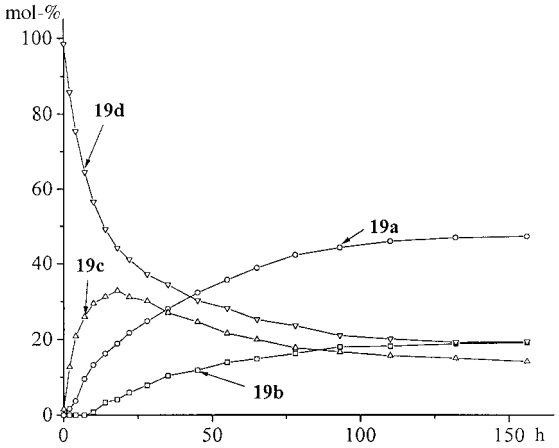

Fig. 12. *Kinetic curves of the thermal isomerization of the pure complex* **19d** (HFB, 85°)

Scheme 9

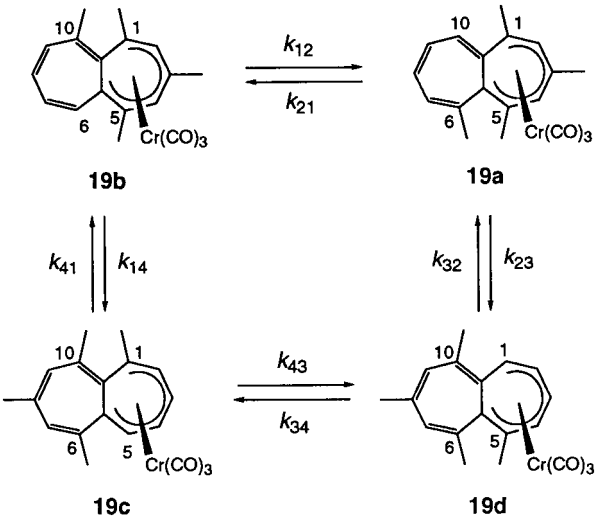

Table 8. *Rate Constants* [s^{-1}] *of the Thermal Rearrangements of Complexes* **19a**–**19d** *at 85° in HFB and Free Activation Energies*[a])

1,2-Intra-ring $Cr(CO)_3$ shift				η^6,η^6-Inter-ring $Cr(CO)_3$ shift			
$K_{12}\cdot 10^5$	$K_{21}\cdot 10^5$	$K_{43}\cdot 10^5$	$K_{34}\cdot 10^5$	$K_{23}\cdot 10^5$	$K_{32}\cdot 10^5$	$K_{41}\cdot 10^5$	$K_{14}\cdot 10^5$
0.49 ± 0.01	0.20 ± 0.01	1.15 ± 0.04	0.81 ± 0.02	0.15 ± 0.002	0.49 ± 0.01	0.15 ± 0.003	0.24 ± 0.003
Calculated Values of Free Activation Energies $\Delta G^{\neq}$ [kcal·mol^{-1}]: $\Delta G^{\neq}=4.576\cdot T\cdot(10.319+\lg T-\lg k)$							
19b → **19a**	**19a** → **19b**	**19c** → **19d**	**19d** → **19c**	**19a** → **19d**	**19d** → **19a**	**19c** → **19b**	**19b** → **19c**
29.8	30.5	29.2	29.4	30.6	29.8	30.7	30.4

[a]) Values of equilibrium constants found: $K_{12}=2.528\pm0.050$; $K_{23}=0.301\pm0.01$; $K_{34}=0.710\pm0.02$; $K_{14}=1.611$ (calc.), $K_{14}=1/K_{12}\cdot)K_{23}\cdot K_{34}$.

haptotropic rearrangement in [$Cr(CO)_3$ (naphthalene)] (**22**; *Scheme 10*). Most probably, a similar type of coordination should be present in the transition state for the inter-ring haptotropic migrations of the $Cr(CO)_3$ group in [$Cr(CO)_3$(heptalene)] (**1**) as the bis-homologue of **22**. Indeed, *Lindner* and co-workers have found by π-SCF force-field calculations that the double-ring inversion of heptalene itself should take place *via* a fully planar transition state [2]. It demands, under the prerequisite that the migration of the $Cr(CO)_3$ group is not accompanied by DBS, η^4-coordination with the heptalene atoms C(1), C(5a), C(10), and C(10a) in the transition state, *i.e.*, the transition state should adopt C_s symmetry as for the $Cr(CO)_3$ group migration in **22**. The migration of the $Cr(CO)_3$ group in **1** is concluded when the $Cr(CO)_3$ group is again η^6-coordinated to the heptalene fragment at the atoms C(6), C(7), C(8), C(9), C(10), and C(10a). To describe the situation in topological terms, it can be said that the $Cr(CO)_3$ group moves diagonally across the heptalene core from one seven-membered ring to the other, thereby avoiding DBS, which would be the result of a lateral migration of the $Cr(CO)_3$ group *via* the η^4-coordinated heptalene fragment, involving the atoms C(5), C(5a), C(6), and C(10a). This process would end with η^6-coordination of the $Cr(CO)_3$ group to the heptalene atoms C(5a), C(6), C(7), C(8), C(9), and C(10) (*cf. Scheme 11*). However, the transition-state situation may become much more complicated in the presence of alkyl substituents in the *peri*-positions of the heptalene ligands in corresponding $Cr(CO)_3$ complexes due to the expected for *peri*-substituents in planar transition states. In such cases, the double ring inversion of the free heptalene ligands takes place *via* non-planar transition states [2][19] (see also Footnote 7 in [16]) that can be described according to *Lindner*'s calculations as double-chair conformations of the heptalene skeleton in which the juxtaposed *peri*-substituents are moved away from each other [2]. However, the torsion angles around the central σ-bond are close to 0° as would be necessary for η^4-coordination of a $Cr(CO)_3$ group in the transition state, which is required for its diagonal movement from one seven-membered ring to the other. The X-ray crystal-structure analysis of **19b**, as well as that of **20b**, also indicates the assumed diagonal movement of the $Cr(CO)_3$ group across the heptalene skeleton during the course of the inter-ring haptotropic rearrangements, because the distance of the Cr-atom to the non-bonded central C-atom in both complexes is only 26% larger than the average Cr–C bond length of the η^6-coordinated π-fragment of the heptalene core. Moreover, the dinuclear complex **20b** can be regarded as an excellent model for the starting and terminal situation of the inter-ring haptotropic shift of the $Cr(CO)_3$ group in complex **19b**. However, the kinetic analyses show that the inter-ring migration of the $Cr(CO)_3$ fragments takes place with DBS (see *Scheme 9*) that requires a lateral movement of the $Cr(CO)_3$ group. Theoretical DFT studies, which are in progress, will give more information about the detailed mechanisms of these rearrangements.

Scheme 10

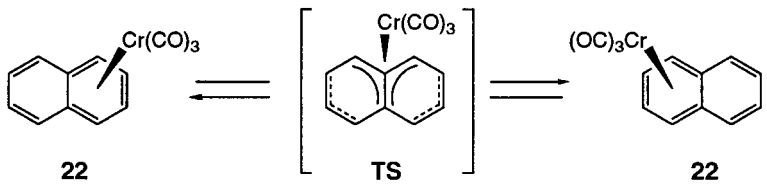

Scheme 11

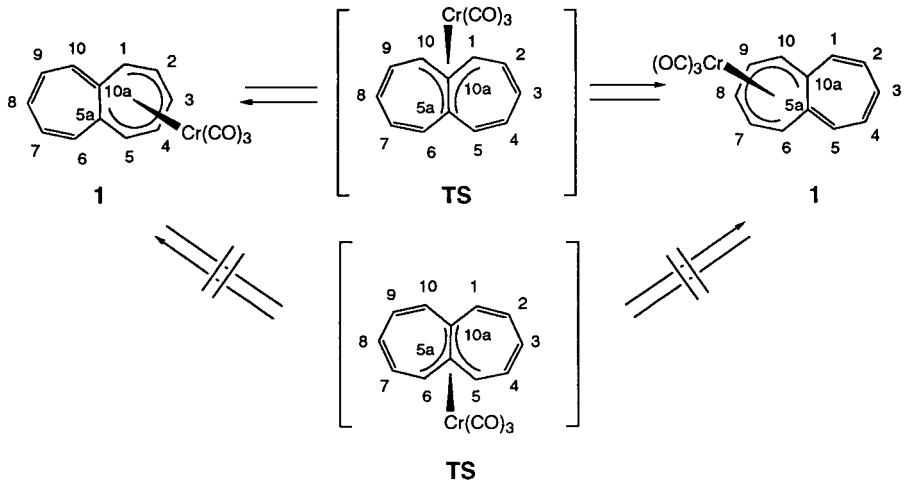

3. Concluding Remarks. – We have demonstrated that $Cr(CO)_3$ complexes of heptalenes undergo two different types of haptotropic rearrangement. These are characterized by an intramolecular 1,2-shift (back and forth movement) of the $Cr(CO)_3$ group within the same seven-membered ring (intra-ring displacement) and accompanied by DBS of the heptalene ligand, and by an intramolecular transannular shift of the $Cr(CO)_3$ group across the central σ-bond between both seven-membered rings (inter-ring displacement) also with DBS of the heptalene ligand. Both rearrangements possess similar free energies of activation, *i.e.*, they take place concomitantly and lead finally to the thermal equilibrium of all four possible isomers of the $Cr(CO)_3$ complexes of unsymmetrically substituted heptalenes.

However, one question has not yet been addressed. Heptalenes are inherently chiral molecules with C_2 symmetry of the relevant heptalene core [22]. This means that the two seven-membered rings, which can be regarded as two intercalated heptafulvene substructures that together build a twisted bowl-like form (*cf. Introduction*), possess homotopic faces. For each ring, these faces are diastereotopic with respect to intermolecular encounters, due to the inherent chirality of the heptalene body. The '*exo*'-face of the twisted bowl-like heptalene core can, therefore, be designated *re* in the case of (*M*)-chirality and *si* in the case of (*P*)-chirality[6]). In turn, the '*endo*'-face has to be designated *si* for (*M*)- and *re* for (*P*)-chirality of the heptalene core. The X-ray crystal structure of **19b** clearly shows that the $Cr(CO)_3$ group is bound to the '*exo*'-face of the more highly substituted ring of **13b** and, as a consequence, the dinuclear complex **20b** carries both $Cr(CO)_3$ groups on the 'homotopic' '*exo*'-sites of **13b**, as is obvious from the X-ray crystal structure of **20b** (*cf. Figs. 7–9*). It seems that '*endo*'-configured $Cr(CO)_3$ complexes of heptalenes, in contrast to the corresponding dinuclear $Fe(CO)_3$

---

[6]) This designation is strictly valid for all substituted heptalenes in which the C_2 symmetry of the parent structure has been preserved. All other substituted heptalenes have no element of symmetry (C_1). The faces on the same side of both rings are diastereotopic, and only the faces of their discussed π-core preserve homotopicity.

complexes [25], are not formed, since they are strongly destabilized by a *cis*-arrangement of the second non-complexed ring, especially with respect to its C(10)=C(10a) bond and the $Cr(CO)_3$ group (*cf.* the similar situation in $Fe(CO)_3$ complexes of heptalenes, *e.g.*, **2** and **3** in *Schemes 2* and *3*). This group can be regarded as a 'face marker' which forbids face interchange (racemization) by double ring inversion, as happens in free heptalene ligands. On the other hand, DBS in complexed heptalenes are the result of back and forth 1,2-migrations of the $Cr(CO)_3$ group, which, in contrast to free heptalene ligands where DBS takes place easily with retention of configuration [16], should occur with inversion of configuration as a result of face fixation through complexation. This signifies racemization for all symmetrically substituted heptalenes with respect to a pseudo-mirror plane passing through C(3), C(8), and the central C(5a)–C(10a) bond (*Scheme 12*)[7]). Therefore, measuring the rate of racemization of optically active $Cr(CO)_3$ complexes of suitably substituted heptalenes, such as **23**, will provide the activation parameters only for the ongoing DBS processes. Experiments in this direction are in progress.

Scheme 12

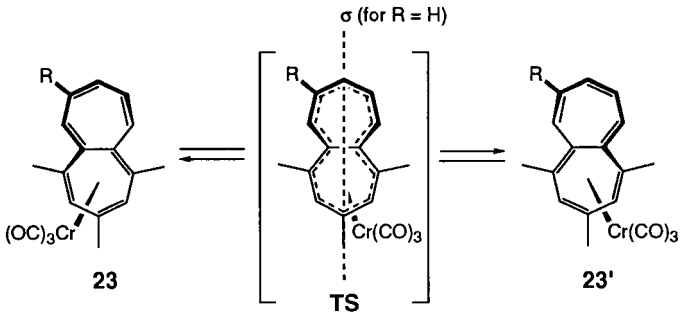

The funding of this work by the *CEEC/NIS* program of the *Swiss National Science Foundation* as well as by *INTAS* (grant No. 94-2921) and by the *Russian Foundation for Basic Research* (No. 96-03-3241) is gratefully acknowledged.

Experimental Part

General. All operations, except TLC, were performed under a purified Ar atmosphere. All solvents (Et_2O, THF, benzene, hexafluorobenzene (HFB), hexane) were purified by refluxing over K/Na alloy and were distilled therefrom under Ar just before use. DME was purified by refluxing over sodium diphenylketyl and was distilled therefrom just before use. Column chromatography (CC) was performed on silica gel *60* (40–63 μm; *Chemie Uetikon AG*). Prep. HPLC was conducted on a *830LC* instrument (*DuPont*) with a *Sperisorb* NH_2 (5 μ) column (20 × 250 mm). Anal. HPLC was conducted on a *991* instrument (*Waters*), equipped with a photo-diode detector array, also with a *Spherisorb* NH_2 column (4.6 × 250 mm). UV Spectra were measured with a *Lambda 9* instrument (*Perkin-Elmer*) or taken as '*ad hoc*' spectra with the photo-diode array detector of the *Waters* instrument. IR Spectra: *UR-20* (*Carl Zeiss*) or FT spectrometer (*Perkin-Elmer*). NMR Spectra: *VXR 400* (*Varian*), and *ARX 300* or *AMX 600* (*Bruker*) spectrometers. Assignments of the signals based on additional COSY, NOESY, and ^1H, ^{13}C correlation spectra (HSQC and HMBC techniques), as well as NOE

---

[7]) The transition state of the DBS process in $Cr(CO)_3$ complexes of heptalenes can be regarded as the complexed C_{2v} transition state of the free heptalene ligands for racemization (*cf.* [16]), which is not followed, because double-ring inversion is energetically more favorable in the free heptalenes.

measurements by the NOEDIF procedure. MS: *MAT 90* instrument (*Finnigan*); if not otherwise stated, in the EI mode at 70 eV.

1. Syntheses of the Heptalenes. – 1.1. *Thermal Equilibrium Mixture of 1,3,5,6- and 1,3,5,10-Tetramethylheptalene* (**13a** and **13b**, resp.). 1.1.1. *Thermal Equilibrium Mixture of Dimethyl 6,8,10-Trimethylheptalene-1,2- and -4,5-dicarboxylate* (**6a** and **6b**, resp.) (*cf.* [2][28][39]). 4,6,8-Trimethylazulene (1.75 g, 10.28 mmol) [40] and ADM (5.7 ml, 6.57 g, 46.25 mmol) were dissolved in MeCN (100 ml; dried over *Alox*), degassed with Ar and transferred under Ar in a *Schlenk* vessel. After stirring and heating at 100° for 24 h, MeCN and the excess ADM were removed by distillation *in vacuo* in a rotatory evaporator. The residue, TLC (silica gel; hexane/Et_2O 3:2) of which indicated the presence of **6a**/**6b** in addition to small amounts of non-reacted azulene and traces of *dimethyl 4,6,8-trimethylazulene-1,2-dicarboxylate* (**7**), as well as slow-moving material (*cf.* [41]), was subjected to CC (hexane/Et_2O 3:2) which gave the pure 1:4 mixture **6a**/**6b** as a red oil (1.55 g, 48%), which was directly reduced in the next step.

1.1.2. *6,8,10-Trimethylheptalene-1,2- and -4,5-dimethanol* (**8a** and **8b**, resp.) (*cf.* [28][42]). The mixture **6a**/**6b** (1.55 g, 4.96 mmol) was dissolved in THF (15 ml) and added dropwise under stirring at 15° to a soln. of 2M DIBAH (15 ml) in THF (100 ml). A conc. aq. soln. of *Seignette* salt was added dropwise under vigorous stirring. Extraction with AcOEt, drying of the org. layers, and distillation in a rotatory evaporator led to a mixture of yellow and orange crystals (0.638 g, 50%). The yellow crystals corresponded to **8b** and the orange ones to **8a**. However, in some cases, we observed that the mixture of crystals contained the yellow form of **8b** in addition to an orange-colored rhombic form, which was found to be *6,10a-dihydro-7,10,10a-trimethyl-2*H*-heptaleno[1,10-*bc*]furan-3-methanol* (**9**[2]). Recrystallization of **9** from acetone/hexane led back to the thermal equilibrium mixture **8a**/**8b**, from which **8b** crystallized preferentially.

Data of **8a**: UV (hexane/5% i-PrOH): λ_{max} 210 (0.80), 258 (1.00), 319 (0.16), long tailing up to 450; λ_{min} 219 (0.49), 295 (0.14). ^{1}H-NMR (300 and 600 MHz, $CDCl_3$; C*H*Cl_3 at 7.260): 6.50 (*dd*, *J* = 11.4, 6.1, H–C(4)); 6.42 (*d*, *J* = 11.4, H–C(3)); 6.12 (br. *s*, H–C(9)); 5.91 (br. *s*, H–C(7)); 5.79 (*d*, *J* = 6.1, H–C(5)); 4.61, 4.05 (*AB*, J_{AB} = 12.8, CH_2–C(1)); 4.49, 4.24 (*AB*, J_{AB} = 11.9, CH_2–C(2)); 2.48, 2.41 (2 br. *s*, OH); 2.09 (*d*, *J* = 1.1, Me–C(6)); 1.96 (*d*, *J* = 1.1, Me–C(8)); 1.64 (*s*, Me–C(10)). ^{13}C-NMR (150.9 MHz, $CDCl_3$; *C*DCl_3 at 77.00): 142.01 (C(5a)); 139.84 (C(2)); 138.34 C(8)); 135.11 (C(6)); 134.18 (C(1)); 132.47 (C(3)); 131.52 (C(4)); 130.81 (C(10)); 129.93 (C(7)); 128.70 (C(10a)); 122.09 (C(5)); 64.20 (*C*H_2–C(1)); 63.49 (*C*H_2–C(2)); 25.42 (*Me*–C(8)); 24.97 (*Me*–C(6)); 18.16 (*Me*–C(10)).

Data of **8b**: UV (hexane/5% i-PrOH). λ_{max} 212 (0.69), 240S (0.80), 257 (1.00), 308 (0.15), long tailing up to 450; λ_{min} 225 (0.51), 294 (0.14). ^{1}H-NMR (300 and 600 MHz, $CDCl_3$; C*H*Cl_3 at 7.260): 6.56 (*d*, *J* = 6.1, H–C(3)); 6.22 (*dd*, *J* = 10.1, 6.1, H–C(2)); 6.07 (br. *s*, H–C(9)); 5.94 (br. *s*, H–C(7)); 5.90 (*d*, *J* = 10.1, H–C(1)); 4.37, 4.30 (*AB*, J_{AB} = 13.0, CH_2–C(5)); 4.36, 4.33 (*AB*, J_{AB} = 11.5, CH_2–C(4)); 2.24 (*s*, 2 OH); 2.12 (*d*, *J* = 1.1, Me–C(6)); 1.97 (br. *s*, Me–C(8)); 1.71 (*s*, Me–C(10)). ^{13}C-NMR (150.9 MHz, $CDCl_3$; C*D*Cl_3 at 77.00): 143.25 (C(4)); 139.52 (C(5a)); 138.82 (C(8)); 133.73 (C(3)); 131.86 (C(5)); 130.81 (C(6)); 130.56 (C(9)); 130.14 (C(7), C(10)); 129.30 (C(2)); 129.13 (C(1)); 126.57 (C(10a)); 67.50 (*C*H_2–C(5)); 59.64 (*C*H_2–C(4)); 25.22 (*Me*–C(6)); 24.72 (*Me*–C(8)); 17.14 (*Me*–C(10)).

Data of **9**: Crystal modification occurred at *ca.* 120° with melting at 129–131° (m.p. of **8b**). ^{1}H-NMR (300 MHz, $CDCl_3$; C*H*Cl_3 at 7.260): 6.26 (*d*, *J* = 9.7, H–C(4)); 6.23 (*s*, H–C(10)); 5.43 (*s*, H–C(8)); 5.41 (*dt*, partially covered, *J* = 9.7, 7.5, H–C(5)); 4.85, 4.81 (*AB*, J_{AB} = 11.9, CH_2(2)); 4.40 (br. *s*, CH_2–C(3)); 2.65, 2.40 (*ABX*, J_{AB} = 12.8, J_{AX} = 7.3, J_{BX} = 7.1, CH_2(6)); 2.14 (*s*, Me–C(7)); 1.82 (Me–C(9)); 1.01 (Me–C(10a)); 1.57 (very br. *s*, presumably OH). ^{13}C-NMR (75 MHz, $CDCl_3$; *C*DCl_3 at 77.00): 19.79 (*Me*–C(10a)); 22.72 (*Me*–C(9)); 24.14 (*Me*–C(7)); 30.08 (C(6)); 64.26 (*C*H_2–C(3)); 68.32 (C(2)); 82.68 (C(10a)); 118.23, 127.03, 131.71, 132.15 (C(4), C(5), C(8), C(10)); 119.85, 130.01, 135.12, 135.72, 136.68, 137.85 (C(2a), C(3), C(6a), C(7), C(9), C(10b)). CI-MS (NH_3): 257.4 (8, $[M+1]^+$), 239.4 (100, $[M+1-H_2O]^+$), 223.3 (2).

1.1.3. *Acid-Catalyzed Disproportionation of* **8b**. To a soln. of **8b** (0.0542 g, 0.213 mmol) in toluene (12 ml), three drops of a 5% soln. of TsOH in acetone were added. The mixture was stirred at 80° for 10 min. The cooled soln. was washed with sat. aq. $NaHCO_3$ soln. and then with H_2O. CC (Et_2O/hexane 4:1) of the residue of the org. phase gave a 5.8:1 pure thermal-equilibrium mixture **10a**/**10b** (0.0367 g, 72%) as an orange oil.

Data of 1,6,8,10-Tetramethylheptalene-2-carbaldehyde (**10a**): ^{1}H-NMR (300 MHz, $CDCl_3$; C*H*Cl_3 at 7.260): 10.16 (*s*, CHO); 6.83 (*d*, *J* = 11.6, H–C(3)); 6.49 (*dd*, *J* = 11.5, 6.0, H–C(4)); 5.79 (*d*, *J* = 6.0, H–C(5)); 6.16 (br. *s*, H–C(9)); 5.92 (br. *s*, H–C(7)); 2.39 (*s*, Me–C(1)); 2.06 (*d*, *J* = 1.2, Me–C(6)); 1.97 (*d*, *J* = 1.3, Me–C(8)); 1.73 (*s*, Me–C(10)). ^{13}C-NMR (75.4 MHz, $CDCl_3$): 190.13 (CHO); 131.33, 130.62, 129.94, 126.38, 122.79 (C(3), C(4), C(5), C(7), C(9)); 25.37, 24.07, 18.85, 18.25 (4 Me).

Data of 5,6,8,10-Tetramethylheptalene-4-carbaldehyde (**10b**): ^{1}H-NMR (300 MHz, $CDCl_3$): 9.53 (*s*, CHO); 7.08 (*d*, *J* = 6.0, H–C(3)); 6.39 (*dd*, *J* = 10.1, 6.0, H–C(3)); 6.21 (*d*, *J* = 10.1, H–C(1)); 6.11 (br. *s*, H–C(9));

6.04 (br. *s*, H–C(7)); 1.95 (*s*, Me–C(5)); 2.01 (*d*, *J* = 1.4, Me–C(6)); 1.96 (*d*, *J* = 1.3, Me–C(8)); 1.70 (*s*, Me–C(10)).

1.1.4. *Thermal Equilibrium Mixture of 1,6,8,10-Tetramethylheptalene-2-methanol* (**11a**) *and 5,6,8,10-Tetramethylheptalene-4-methanol* (**11b**). The 2:1 thermal-equilibirum mixture **8a**/**8b** (0.197 g, 0.765 mmol) was disproportionated in toluene (45 ml) as described above. The isolated mixture **10a**/**10b** was reduced to **11a**/**11b** with DIBAH in THF (30 ml) at 0°. Workup with aq. *Seignette*-salt soln. and CC (Et_2O/hexane 3:2) gave the pure 3.3:1 thermal-equilibrium mixture of **11a**/**11b** (0.150 g, 81% with respect to the mixture **8a**/**8b**) as an orange oil.

Data of **11a**: ^{1}H-NMR (300 MHz, $CDCl_3$; C*H*Cl_3 at 7.260): 6.44 (*A* of *ABX*, $^3J_{AB}$ = 4.7, $^4J_{AX}$ = 1.9, H–C(5)); 6.42 (*B* of *ABX*, $^3J_{AB}$ = 4.7, $^3J_{BX}$ = 12.0, H–C(4)); 6.13 (br. *s*, H–C(9)); 5.91 (*quint.*-like, *J* = 1.4, H–C(7)); 5.74 (*X* of *ABX*, $^4J_{AX}$ = 1.9, $^3J_{BX}$ = 12.0, H–C(3)); 4.40, 4.28 (*AB*, J_{AB} = 11.8, CH_2–C(2)); 2.06 (*d*, *J* = 1.3, Me–C(6)); 2.02 (*s*, Me–C(1)); 1.96 (*d*, *J* = 1.3, Me–C(8)); 1.68 (*s*, Me–C(10)); 1.5 (very br. *s*, OH).

Data of **11b**: ^{1}H-NMR (300 MHz, $CDCl_3$; C*H*Cl_3 at 7.260): *ca.* 6.43 (*d*, *J* = 6.2, H–C(3)); 6.16 (*dd*, *J* = 10.2, 6.2, H–C(2)); 6.04 (br. *s*, H–C(9)); 5.93 (br. *s*, H–C(7)); 5.87 (*d*, *J* = 10.1, H–C(1)); 4.70, 4.20 (*AB*, J_{AB} = 13.0, CH_2–C(4)); 1.99 (*d*, *J* = 1.3, Me–C(6)); 1.97 (*d*, *J* = 1.3, Me–C(8)); 1.81 (*s*, Me–C(10)); 1.70 (*d*, *J* = 0.7, Me–C(5)); 1.5 (very br. *s.*, OH).

All attempts to reduce the mixture **11a**/**11b** with Et_3SiH in TFA at 60° (*cf.* [29]) failed completely. Dissolution of **11a**/**11b** (0.075 g, 0.312 ml) in TFA (1.5 ml) at r.t. led at once to a brown colored soln. Addition of Et_3SiH (0.3 ml) and heating at 60° for 4 h did not yield the expected mixture of pentamethylheptalenes **12a**/**12b**. No product with UV absorption at 254 nm could be isolated after the usual workup procedure.

Treatment of the mixture of **11a**/**11b** with MnO_2 (*cf.* [30]) in CH_2Cl_2 at 20° gave back the 5.8:1 mixture of the aldehydes **10a**/**10b**.

1.1.5. *Decarbonylation of the 5.8:1 Mixture* **10a**/**10b**. The 2:1 thermal-equilibrium mixture **8a**/**8b** (0.730 g, 2.848 mmol) was disproportionated to the corresponding 5.8:1 mixture **10a**/**10b** (*ca.* 0.500 g after CC), which was dissolved in toluene (40 ml). The *Wilkinson* catalyst [$Rh(Ph_3P)_3Cl$] (2.10 g, 2.27 mmol) was added. The mixture transferred in a *Schlenk* vessel under Ar and stirred at 120° for 3 h. After cooling, hexane (80 ml) was added, the soln. was filtered, and the solvents were distilled off. A first CC (*Alox B*, act. IV; hexane) gave the thermal 4:1 equilibrium mixture of the tetramethylheptalenes **13a**/**13b** (0.156 g, 35%) as an orange oil and, in a second fraction, Ph_3P (0.281 g).

Data of **13a**: UV (hexane): λ_{max} 208 (0.70), *ca.* 240 (sh, 0.89), 252 (1.00), 318 (0.17), long tailing up to 450; λ_{min} 225 (0.49), 289 (0.13). ^{1}H-NMR (600 MHz, $CDCl_3$; C*H*Cl_3 at 7.260): 6.379 (*dd*, *J* = 11.0, 6.2, H–C(9)); 6.286 (*dd*, *J* = 11.1, 5.9, H–C(8)); 6.154 (*d* with fine structure, *J* = 5.8, H–C(7)); 6.119 (br. *s*, H–C(4)); 5.905 (*quint.*-like, *J* = 1.3, H–C(2)); 5.713 (*d*, *J* = 6.1, H–C(10)); 2.063 (*d*, *J* = 1.2, Me–C(1)); 2.021 (br. *s*, Me–C(6)); 1.964 (*d*, *J* = 1.2, Me–C(3)); 1.720 (*s*, Me–C(5)). ^{13}C-NMR (150.9 MHz, $CDCl_3$; *C*Cl_3 at 77.00): 139.53 (C(10a)); 138.01 (C(3)); 135.15 (C(1)); 133.58 (C(6)); 131.79 (C(4)); 130.62 (C(5a)); 129.77 (C(2)); 129.58 (C(8)); 129.47 (C(5), C(9)); 127.21 (C(7)); 122.32 (C(10)); 25.39 (*Me*–C(3)); 24.54 (*Me*–C(1)); 23.08 (*Me*–C(6)); 18.44 (*Me*–C(5)).

Data of **13b**: UV (hexane): λ_{max} 205 (0.95), 243 (sh, 0.83), 255 (1.00), 312 (0.14), long tailing up to 450; λ_{min} 224 (0.47), 290 (0.13). ^{1}H-NMR (600 MHz, $CDCl_3$; C*H*Cl_3 at 7.260): 6.389 (*d*, *J* = 10.9, H–C(9)); 6.303 (*dd*, *J* = 10.9, 5.9, H–C(8)); 6.166 (*dd*, *J* = 10.1, 5.9, H–C(7)); 6.080 (br. *s*, H–C(4)); 5.942 (br. *s*, faintly *quint.*-like, H–C(2)); 5.782 (br. *d*, *J* = 10.1, H–C(6)); 1.987 (*d*, *J* = 1.2, Me–C(1)); 1.970 (br. *s*, Me–C(3)); 1.752 (*s*, Me–C(10)); 1.715 (br. *s*, Me–C(5)). ^{13}C-NMR (150.9 MHz, $CDCl_3$; *C*Cl_3 at 77.00): 138.54 (C(3)); 136.78 (C(10)); 135.77 (C(10a)); 133.21 (C(1)); 130.71 (C(4)); 130.21 (C(2)); 129.84 (C(8)); 129.58 (C(9)); 129.28 (C(5)); 128.96 (C(7)); 128.87 (C(5a)); 127.20 (C(6)); 24.92 (*Me*–C(3)); 23.37 (*Me*–C(1)); 18.40 (*Me*–C(10)); 17.06 (*Me*–C(5)).

1.2. *4,6,7,9,11-Pentamethylheptaleno[1,2-c]furan* (**16**). 1.2.1. *Dimethyl 1,3,6,8,10-Pentamethylheptalene-4,5-dicarboxylate* (**14b**). Dicarboxylate **14b** was prepared according to [12] by an improved procedure [43] in 20–30% yield after CC and crystallization from Et_2O/hexane. M.p. 144–146°.

1.2.2. *1,3,6,8,10-Pentamethylheptalene-4,5-dimethanol* (**15b**). Dicarboxylate **14b** (0.370 g, 1.087 mmol) was dissolved in THF and added dropwise to a soln. of DIBAH in THF at 0°. The usual workup gave **15b**, after CC and crystallization in pure form (0.275 g, 89%).

Data of **15b**: M.p. 194° (AcOEt). UV (hexane/7% i-PrOH): λ_{max} 211 (0.79), 256 (1.00), 305 (0.15); λ_{min} 230 (0.62), 297 (0.15). IR ($CHCl_3$): 3597*m* (free OH), 3470*m* (bound OH), 3003*s*, 2968*m*, 2943*m*, 2914*m*, 1649*w*, 1624*w*, 1599*w*, 1440*m*, 1376*m*, 1010*m*, 988*s*, 860*m*, 845*m*. ^{1}H-NMR (300 MHz, $CDCl_3$; C*H*Cl_3 at 7.260): 6.05 (br. *s*, H–C(2), H–C(9)); 5.94 (br. *s*, H–C(7)); 4.41, 4.32 (*AB*, J_{AB} = 11.9, CH_2–C(4)); 4.43, 4.40 (*AB*, J_{AB} = 13.1, CH_2–C(5)); 2.12 (*s*, Me–C(3)); 2.10 (*d*, *J* = 1.3, Me–C(6)); 1.974 (*d*, *J* = 1.5, Me–C(1)); 1.968 (*d*, *J* = 1.5,

Me–C(8)); 1.93 (br. *s*, 2 OH); 1.71 (*s*, Me–C(10)). CI-MS (NH_3): 285.2 (2, $[M+1]^+$), 267.2 (100, $([M+1]-H_2O]^+$), 251.2 (2.5). Anal. calc. for $C_{19}H_{24}O_2$ (284.40): C 80.24, H 8.51; found: C 80.32, H 8.43.

Heating **15b** in toluene at 110° gave rapidly an equilibrium mixture of **15b** and its DBS isomer *3,5,6,8,10-pentamethylheptalene-1,2-dimethanol* (**15a**) in a ratio of 1:2.

Data of **15a**: M.p. 148° (Et_2O). UV (hexane/7% i-PrOH): Almost identical with that of **15b**. IR ($CHCl_3$): 3605*m* (free OH), 3443*m* (bound OH), 2999*s*, 2974*s*, 2943*s*, 2916*s*, 2861*m*, 1649*w*, 1608*m*, 1441*m*, 1375*m*, 1028*m*, 990*s*, 861*m*, 846*m*. ^{1}H-NMR (300 MHz, $CDCl_3$; C*H*Cl_3 at 7.260): 6.21 (*d*-like, $J\approx1$, H–C(4)); 6.09 (br. *s*, H–C(9)); 5.98 (*quint.*-like, H–C(7)); 4.49, 4.20 (*AB*, $J_{AB}=12.4$, CH_2–C(1)); 4.42 (*s*, CH_2–C(2)); 2.12 (*d*, $J=1.3$, Me–C(3)); 2.00 (*d*, $J=1.3$, Me–C(6)); 1.98 (*d*, $J=1.2$, Me–C(8)); 1.71 (*s*, Me–C(5)); 1.68 (*s*, Me–C(10)). CI-MS (NH_3): 285.2 (4.5, $[M+1]^+$), 284.2 (8, $M^{+\cdot}$), 267.2 (100, $([M+1]-H_2O)^+$). Anal. calc. for $C_{19}H_{24}O_2$ (284.40): C 80.24, H 8.51; found: C 79.86, H 8.58.

1.2.3. *Dehydrogenation of* **15b** *with* MnO_2. Dimethanol **15b** (0.275 g, 0.967 mmol) was dissolved in CH_2Cl_2 (50 ml), and MnO_2 (basic [44]; 5.5 g) was added. The mixture was vigorously stirred during 40 min at ambient temp., and MnO_2 was then removed by filtration over *Celite*. Six drops of TsOH (1%) in acetone were added, and the mixture was left at ambient temp. for additional 2 h. After this time, the CH_2Cl_2 soln. was washed with aq. $NaHCO_3$ soln. and H_2O. The residue of the CH_2Cl_2 phase was subjected to CC (hexane/Et_2O 3:2). A first fraction contained **16** (0.137 g, 53.5%; 0.095 g, 37%[8]) a second *4,6,7,9,11-pentamethylheptaleno[1,2-*c*]furan-3(1*H*,3*H*)-one* (**18a**; 0.028 g, 10%; 0.017 g, 6.2%), and a third *4,6,7,9,11-pentamethylheptaleno[1,2-*c*]furan-1(1*H*,3*H*)-one* (**17a**: 0.064 g, 23.5%; 0.050 g, 18.5%)[5]).

Data of **16**: Light-yellow crystals (hexane). M.p. 137.3–138.0°. R_f (Et_2O/hexane 3:2) 0.64. UV (hexane): λ_{max}: 373 (2.89), 321.6 (3.78), with long tailing up to 450, 275.0 (4.18), 237S (4.16), 216 (4.39), 210 (4.39); λ_{min} 308.5 (3.75), 253.7 (4.04), 213 (4.39). IR ($CHCl_3$): 2999*s*, 2942*s*, 2915*s*, 2883*m*, 2857*s*, 2729*w*, 1748*w*, 1624*s*, 1449*s*, 1440*s*, 1375*s*, 1262*m*. ^{1}H-NMR (300 MHz, $CDCl_3$; C*H*Cl_3 at 7.260): 7.488 (*d*, $J=1.6$, H–C(3)); 7.125 (*d*, $J=1.7$, H–C(1)); 6.110 (br. *s*, H–C(10)); 6.009 (*quint.*-like, H–C(8)); 5.785 (*q*-like, $J=1.4$, H–C(5)); 2.126 (*d*, $J=1.4$, Me–C(4)); 1.992 (*d*, $J=1.3$, Me–C(9)); 1.942 (*d*, $J=1.4$, Me–C(7)); 1.844 (*s*, Me–C(11)); 1.716 (*s*, Me–C(6)). EI-MS: 264 (100, $M^{+\cdot}$), 249 (75), 234 (18), 223 (32), 210 (23), 206 (12), 189 (11), 165 (16).

Data of **18a**: Orange-red crystals (AcOEt/hexane). M.p. 203.5–204.3°. R_f (hexane/Et_2O 3:2) 0.34. UV (hexane): λ_{max} 401 (very br., 2.95), 316 (sh, 3.59), 269 (4.37), 240 (4.23), 205 (4.39); λ_{min} 376 (2.94), 248 (4.20), 224.5 (4.16). IR ($CHCl_3$): 302*m*, 2937*m*, 2918*m*, 1754/1743*s*, 1630*w*, 1600*w*, 1524*w*, 1450*m*, 1376*w*, 1342*m*, 1284*w*. ^{1}H-NMR (300 MHz, $CDCl_3$; C*H*Cl_3 at 7.260): 6.473 (*q*-like, $J=1.3$, H–C(5)); 6.102 (br. *s*, H–C(10)); 5.976 (br. *s*, H–C(8)); 4.987, 4.838 (*AB*, $J_{AB}=16.8$, CH_2(3)); 2.029 (*d*, $J=1.3$, Me–C(5)); 1.973 (*d*, $J=1.2$, Me–C(9)); 1.935 (*d*, $J=1.2$, Me–C(7)); 1.745 (*s*, Me–C(6)); 1.673 (*s*, Me–C(11)). EI-MS: 280 (100, $M^{+\cdot}$), 265 (30), 240 (46), 226 (77), 221 (29), 165 (17).

Data of **17a**: Light-red crystals (AcOEt/hexane). M.p. 204.3–205.5°. R_f (hexane/Et_2O 3:2) 0.46. UV (hexane): λ_{max} 373S (2.89), 312 (3.61), 262 (4.36), 241 (sh, 4.19), 209.5 (4.33); λ_{min} 300.5 (3.60), 228.5 (4.04). IR ($CHCl_3$): 3002*m*, 2947*m*, 2918*m*, 2860*w*, 1759*s*, 1626*m*, 1607*w*, 1440*m*, 1408*w*, 1376*m*, 1342*m*, 1326*m*, 1284*m*. ^{1}H-NMR (600 MHz, $CDCl_3$; C*H*Cl_3 at 7.260): 6.294 (*q*-like, $J\approx1.1$, H–C(5)); 6.069 (br. *s*, H–C(10)); 5.970 (*quint.*-like, H–C(8)); 5.026/4.529 (*AB*, $J_{AB}=17.8$, CH_2(1)); 2.291 (*d*, $J=1.3$, Me–C(4)); 1.986 (*d*, $J=1.1$, Me–C(9)); 1.938 (*d*, $J=1.2$, Me–C(7)); 1.756 (*s*, Me–C(11)); 1.715 (*s*, Me–C(6)). EI-MS: 280 (100, $M^{+\cdot}$), 265 (27), 240 (50), 226 (52), 221 (12), 211 (14), 197 (6), 165 (8).

2. Formation of the $Cr(CO)_3$ Complexes. – 2.1. *Reaction of the Thermal-Equilibrium Mixture* **13a**/**13b** *with* $[Cr(CO)_3(NH_3)_3]$. The mixture **13a**/**13b** (0.16 g, 0.76 mmol) and $[Cr(CO)_3(NH_3)_3]$ (0.15 g, 0.80 mmol) was heated at reflux in DME (15 ml) for 2 h. The solvent was removed *in vacuo* and the residue chromatographed on silica gel. A small amount of the pale-yellow mixture **13a**/**13b** (0.02 g; ratio 3.7:1) was eluted first with petroleum ether/benzene 4:1. When the eluant was changed to petroleum ether/benzene 3:1, a red mixture of the mononuclear complexes **19a**–**19d** followed (0.22 g, 83%). ^{1}H-NMR Analysis indicated a ratio of 1:2.47:2.63:1 for the four complexes. A change of the composition of the eluant mixture to 2:1 allowed the collection of the mixture of the dinuclear complexes **20a** and **20b** (0.04 g, 12.7%) in a ratio of 0.7:1 (^{1}H-NMR). This last fraction also contained a small amount (0.01 g) of $[Cr(CO)_5(NH_3)]$.

2.1.1. *Separation of the Mixture of* $Cr(CO)_3$ *Complexes.* The mononuclear complexes **19a**–**19d** showed on the anal. *Spherisorb* NH_2 column (hexane; flow rate: 1 ml/min) the following t_R values (min): 10.67 (**19b**), 11.44 (**19a**), 12.26 (**19d**), and 13.68 (**19c**) (*cf. Fig. 2*). The dinuclear complexes remained on the column under these

---

[8]) Second values in parentheses refer to the yields of recrystallized material.

conditions. However, with hexane/CH_2Cl_2 3:1 and a flow rate of 1 ml/min, the following t_R values were observed: 7.59 (**20b**) and 7.94 (**20a**).

For the prep. separations, an oily mixture of all six complexes (*ca.* 35 mg), from which some crystalline material, mainly consisting of **19b** and **19d**, had deposited, was injected into the prep. *Spherisorb* NH_2 column in two portions, and eluted with hexane and a flow rate of 10 ml/min. This led to pure, crystalline **19b** (10.6 mg), **19a** (7.9 mg), **19d** (3.2 mg), and **19c** (7.5 mg). The separation of the remaining dinuclear complexes, which were washed from the column with CH_2Cl_2 and reinjected and resolved with hexane/CH_2Cl_2 3:1 as eluent using a flow rate of 10 ml/min, gave **20b** (2.3 mg) and **20a** (2.7 mg) in a pure crystalline form.

Data of Tricarbonyl[(1,2,3,4,5,5a-η)-1,3,5,6-tetramethylheptalene]chromium (**19a**): Wine-red crystals. UV: see *Table 2*. IR (THF): 1974, 1905, 1890 (CO). ^{1}H-NMR: see *Table 3*.

Data of Tricarbonyl[(1,2,3,4,5,5a-η)-1,3,5,10-tetramethylheptalene]chromium (**19b**): Violet crystals. UV: see *Table 2*. IR (THF): 1974, 1905, 1890 (CO). ^{1}H-NMR: see *Table 3*. The structure of **19b** was confirmed by an X-ray crystal-structure analysis (see *Sect. 3* as well as *Figs. 6* and *7*).

Data of Tricarbonyl[(1,2,3,4,5,5a)-η)-1,6,8,10-tetramethylheptalene]chromium (**19c**): Wine-red crystals. UV: see *Table 2*. IR (THF): 1974, 1905, 1890 (CO). ^{1}H-NMR: see *Table 3*.

Data of Tricarbonyl[(1,2,3,4,5,5a-η)-5,6,8,10-tetramethylheptalene]chromium (**19d**): Wine-red crystals. UV: see *Table 2*. IR (THF): 1974, 1905, 1890 (CO). ^{1}H-NMR: see *Table 3*.

Data of cis-*[(1,2,3,4,5,5a-η:6,7,8,9,10,10a-η)-1,3,5,6-tetramethyl heptalene]bis[tricarbonylchromium]* (**20a**): Red crystals. M.p. 157–158° (Et_2O/hexane). UV: see *Table 2*. IR (CH_2Cl_2/THF, resp.): 1987/1995, 1960/1970, 1916(sh)/–, 1890/1890 (CO). ^{1}H-NMR: see *Table 3*.

Data of cis-*[(1,2,3,4,5,5a-η:6,7,8,9,10,10a-η)-1,3,5,10-tetramethylheptalene]bis[tricarbonylchromium]* (**20b**): Red crystals. M.p. 161–164° (Et_2O/hexane). UV: see *Table 2*. IR (CH_2Cl_2/THF, resp.): 1989/1995, 1961/1970, 1923(sh)/–, 1893/1890 (CO). ^{1}H-NMR: see *Table 3*.

The structure of **20b** was confirmed by X-ray crystal-structure analysis (see *Sect. 3* as well as *Fig. 8*).

2.1.2. *Thermal Isomerization of Complexes* **19a**–**19d**. A small amount (0.010 g) of each complex was placed in a 5-mm NMR-sample tube, and the tube was evacuated (10^{-5} mm). HFB (0.4 ml) was condensed from a reservoir with a K mirror into the tube, freeze-pump-thaw cycles were repeated three times on the vacuum line and the tube was then sealed. All four sample tubes were placed in a thermostat at 85.0° (temp. deviations ±2°). After corresponding time intervals, the tubes were cooled rapidly to ambient temp., and ^{1}H-NMR analyses were performed with the *VXR 400* instrument. The signals of the Me groups of **19a**–**19d** (*cf. Table 3*) were well resolved and used for integration. The development of the thermal isomerizations is depicted in *Figs. 9–12*.

The data were analyzed with the KINETICS-2 software, testing seven different kinetic schemes. All 16 kinetic curves were processed simultaneously.

2.2. *Reaction of Heptaleno[1,2-*c*]furan* **16** *with* $[Cr(CO)_3(NH_3)_3]$. A mixture of **16** (0.064 g, 0.024 mmol) and $[Cr(CO)_3(NH_3)_3]$ (0.045 g, 0.024 mmol) was heated at reflux in DME (12 ml) for 2 h. The solvent was distilled off *in vacuo* and the residue chromatographed on silica gel with petroleum ether/benzene 7:1, which gave recovered **16** (0.043 g, 67%). Red complex **21** (0.02 g, 62.5% with respect to reacted **16**) was eluted afterwards with ether/benzene (3:1).

*Data of Tricarbonyl[(7,8,9,10,11,11a-η)-4,6,7,9,11-pentamethylheptaleno[1,2-*c*]furan]chromium* (**21**): Red crystals (hexane). M.p. 158–160° (dec.). IR (THF): 1972, 1903, 1888 (CO). ^{1}H-NMR (400 MHz, C_6D_6): 7.160 (*s*, H–C(1)); 7.495 (*s*, H–C(3)); 5.460 (br. *s*, H–C(5)); 5.407 (br. *s*, H–C(10)); 4.856 (br. *s*, H–C(8)); 2.440 (br. *s*, Me–C(9)); 2.060 (br. *s*, Me–C(4)); 2.010 (br. *s*, Me–C(7)); 1.982 (*s*, Me–C(11)); 1.504 (*s*, Me–C(6)).

3. Crystal-Structure Determinations of 19b and 20b[9]). – All measurements were conducted on a *Rigaku AFC5R* diffractometer with graphite-monochromated MoK_α radiation ($\lambda = 0.71069$ Å) and a 12-kW rotating anode generator. The intensities were collected using $\omega/2\theta$ scans. Three standard reflections, which were measured after every 150 reflections, remained stable throughout each data collection. The intensities were corrected for *Lorentz* and polarization effects. For **19b**, an empirical absorption correction based on the ψ-scans of three reflections was applied [45], while an analytical absorption correction was applied for **20b** [46]. Each structure was solved by SHELXS86 [47]. Direct methods revealed the positions of all non-H-atoms of **19b**, while, for **20b**, the *Patterson* method revealed the positions of the Cr-atoms and all remaining non-H-atoms were

---

[9]) Crystallographic data (excluding structure factors) for the structures of complexes **19b** and **20b** have been deposited with the *Cambridge Crystallographic Data Centre* as deposition No. CCDC-132535 and CCDC-132563, respectively. Copies of the data can be obtained, free of charge, on application to the CCDC, 12 Union Road, Cambridge CB2 1EZ, UK (fax: +44-(0)1223-336033, e-mail: deposit@ccdc.cam.ac.uk).

located in a *Fourier* expansion of the *Patterson* solution. The non-H-atoms were refined anisotropically. All H-atoms were fixed in geometrically calculated positions (d(C–H) = 0.95 Å), and they were assigned fixed isotropic displacement parameters with a value equal to $1.2U_{eq}$ of the parent C-atom. Corrections for secondary extinction were not applied. All refinements were carried out on F using full-matrix least-squares procedures which minimized the function $\Sigma w(|F_o|-|F_c|)^2$, where $w=[\sigma^2(F_o)+(0.005F_o)^2]^{-1}$. The data collection and refinement parameters for each compound are listed in *Table 9*. Neutral atom scattering factors for non-H-atoms were taken from [48a] and the scattering factors for H-atoms from [49]. Anomalous dispersion effects were included in F_c [50]; the values for f' and f'' were taken from [48b]. All calculations were performed by the TEXSAN [51] crystallographic software package and the figures were produced with ORTEPII [52].

Table 9. *Crystallographic Data for Compounds* **19b** *and* **20b**

	19b	**20b**
Crystallized from	benzene/heptane	benzene/heptane
Empirical formula	$C_{19}H_{18}CrO_3$	$C_{22}H_{18}Cr_2O_6$
Formula weight [g mol^{-1}]	346.35	482.37
Crystal color, habit	violet, tablet	ruby, plate
Crystal dimensions [mm]	0.12 × 0.25 × 0.38	0.08 × 0.23 × 0.35
Temp. [K]	173(1)	291(1)
Crystal system	monoclinic	monoclinic
Space group	$P2_1/n$	$P2_1/n$
Z	4	4
Reflections for cell determination	25	25
2θ Range for cell determination [°]	31–39	36–40
Unit-cell parameters a [Å]	11.169(2)	10.657(2)
b [Å]	12.724(3)	13.378(3)
c [Å]	11.413(1)	15.073(2)
β [°]	92.96(1)	102.37(1)
V [Å^3]	1619.9(5)	2099.2(7)
D_{calc} [g cm^{-3}]	1.420	1.526
μ(MoK_α) [mm^{-1}]	0.718	1.071
2θ(max) [°]	55	55
Transmission factors (min; max)	0.924; 1.000	0.741; 0.929
Total reflections measured	4079	5286
Symmetry-independent reflections	3717	4812
Reflections used [$I>2\sigma(I)$]	2618	2975
Parameters refined	208	272
R	0.0418	0.0647
wR	0.0368	0.0520
Goodness of fit s	1.693	2.443
Final Δ_{max}/σ	0.0005	0.0003
$\Delta\rho$ (max; min) [e Å^{-3}]	0.34; –0.47	1.14; –0.85
σ(d(C–C)) [Å]	0.004	0.006–0.008

The quality of the crystals of **20b** was generally quite poor, with several crystals yielding split and broadened reflection profiles. Data were collected from three different crystals and the best data set, which showed the best reflections profiles, was used for the structure refinement. The data quality has resulted in slightly elevated values for the R factors and the standard uncertainties for the atomic parameters.

REFERENCES

[1] L. A. Paquette, *Israel J. Chem.* **1980**, *20*, 233.
[2] K. Hafner, G. L. Knaup, H. J. Lindner, *Bull. Soc. Chim. Jpn*. **1988**, *61*, 155.

[3] P. Kouroupis, H.-J. Hansen, *Helv. Chim. Acta* **1995**, *78*, 1247; K. Abou-Hadeed, H.-J. Hansen, *ibid*. **1997**, *80*, 2535.
[4] A. A. S. Briquet, P. Uebelhart, H.-J. Hansen, *Helv. Chim. Acta* **1996**, *79*, 2282; S. El Houar, H.-J. Hansen, *ibid*. **1997**, *80*, 253.
[5] M. Bühl, H.-J. Hansen, unpublished results.
[6] J. Stegemann, H. J. Lindner, *Tetrahedron Lett*. **1977**, 2515.
[7] H. J. Lindner, B. Kitsche, *Angew. Chem*. **1976**, *88*, 123; *ibid. Int. Ed. Engl*. **1976**, *15*, 106.
[8] J. Song, H.-J. Hansen, unpubl. results J. Song, Ph.D. Thesis, University of Zurich, **1999**.
[9] S. Maillefer, H.-J. Hansen, *Helv. Chim. Acta* **1999**, *82*, in preparation; S. Maillefer, Ph. D. Thesis, University of Zurich, 1998.
[10] M. Bühl, P. Uebelhart, H.-J. Hansen, *Helv. Chim. Acta* **1999**, *82*, in preparation.
[11] H. Kandler, A. J. Rippert, H.-J. Hansen, unpublished results; A. J. Rippert, Ph.D. Thesis, University of Zurich, 1994.
[12] Y. Chen, R. W. Kunz, P. Uebelhart, R. H. Weber, H.-J. Hansen, *Helv. Chim. Acta* **1992**, *75*, 2447.
[13] Y. Chen, Ph. D. Thesis, University of Zurich, 1993.
[14] K. Hafner, G. L. Knaup, H. J. Lindner, H.-C. Flöter, *Angew. Chem*. **1985**, *97*, 209; *ibid., Int. Ed. Engl*. **1985**, *24*, 212.
[15] W. Bernhard, H.-R. Zumbrunnen, H.-J. Hansen, *Chimia* **1979**, *33*, 324; W. Bernhard, P. Brügger, J. J. Daly, G. Englert, P. Schönholzer, H.-J. Hansen, *Helv. Chim. Acta* **1985**, *68*, 1010.
[16] W. Bernhard, P. Brügger, P. Schönholzer, R. H. Weber, H.-J. Hansen, *Helv. Chim. Acta* **1985**, *68*, 429.
[17] E. Vogel, H. Königshofen, J. Wassen, K. Müllen, J. F. Oth, *Angew. Chem*. **1974**, *86*, 777; *ibid., Int. Ed. Engl.* **1974**, *13*, 732.
[18] L. A. Paquette, *Pure & Appl. Chem.* **1982**, *54*, 987; L. A. Paquette, M. P. Trova, J. Luo, A. E. Clough, L. B. Anderson, *J. Am. Chem. Soc*. **1990**, *112*, 228; L. A. Paquette, T.-Z. Wang, J. Luo, C. E. Cottrell, A. E. Clough, L. B. Anderson, *ibid*. **1990**, *112*, 239.
[19] R. Knecht, R. W. Kunz, H.-J. Hansen, unpublished results; R. Knecht, Diploma Thesis, University of Zurich, 1995.
[20] E. Vogel, D. Kerimis, N. T. Allison, R. Zellerhoff, J. Wassen, *Angew. Chem.* 1979, *91*, 579; *ibid., Int. Ed. Engl*. **1979**, *18*, 545.
[21] K. Hafner, G. L. Knaup, *Tetrahedron Lett*. **1986**, *27*, 1665.
[22] W. Bernhard, P. Brügger, J. J. Daly, P. Schönholzer, R. H. Weber, H.-J. Hansen, *Helv. Chim. Acta* **1985**, *68*, 415.
[23] J. Stegemann, H. J. Lindner, *J. Organomet. Chem*. **1979**, *166,* 233.
[24] K. Müllen, N. T. Allison, J. Lex, H. Schmickler, E. Vogel, *Tetrahedron* **1987**, *43*, 3225.
[25] F. W. Grimm, K. Hafner, H. J. Lindner, *Chem. Ber.* **1996**, *129*, 1569.
[26] Y. A. Ustynyuk, O. I. Trifonova, A. V. Yatsenko, A. A. Borisenko, H.-J. Hansen, P. Uebelhart, *Russ. Chem. Bull*. **1994**, *43*, 2100.
[27] J. P. Collman, L. S. Hegedus, J. R. Norton, R. G. Finke, Principles and Applications of Organotransition Metal Chemistry, University Science Books, Mill Valley, CA, 1987; The chemistry of the metal-carbon bond, Vol. 2 – 4; especially Vol. 4, The use of organometallic compounds, F. R. Hartley, ed., John Wiley & Sons, Chichester, 1985 – 1989.
[28] K. Hafner, N. Hock, G. L. Knaup, K.-P. Meinhardt, *Tetrahedron Lett*. **1986**, *27*, 1669; G. L. Knaup, Ph. D. Thesis, Technical University of Darmstadt, 1985.
[29] R. A. Fallahpour, H.-J. Hansen, *Helv. Chim. Acta* **1992**, *75*, 2210.
[30] P. Uebelhart, P. Mohler, R.-A. Fallahpour, H.-J. Hansen, *Helv. Chim. Acta* **1995**, *78*, 1437.
[31] D. B. Dess, J. C. Martin, *J. Am. Chem. Soc*. **1991**, *113*, 7277.
[32] C. Hörndler, H.-J. Hansen, *Helv. Chim. Acta* **1997**, *80*, 2520.
[33] M. D. Rausch, G. A. Moser, E. J. Zaiko, *J. Organomet. Chem.* **1970**, *23*, 185.
[34] T. L. Pauson, K. H. Todd, *J. Chem. Soc*. (C), **1970**, 2315; M. J. Barrow, O. S. Mills, *J. Chem. Soc., Chem. Commun*. **1971**, 119.
[35] a) Yu. F. Oprunenko, S. G. Malyugina, V. A. Roznyatovsky, V. I. Mstislavsky, N. G. Akhmedov, D. N. Laikov, Yu. A. Ustynyuk, Abstr. of XVIII International Conf. in Organometallic Chemistry, Munich, 16 – 21 Aug., 1998, Part II, B. 19; b) Yu. F. Oprunenko, S. Malyugina, Yu. A. Ustynyuk, O. Malyshev, *ibid.*, B. 20.
[36] N. G. Akhmedov, S. G. Malyugina, V. I. Mstislavsky, Yu. F. Oprunenko, V. A. Roznyatovsky, Yu. A. Ustynyuk, A. S. Batsanov, N. A. Ustynyuk, *Organometallics* **1998**, *17*, 4607.

[37] V. G. Gozsky, E. A. Katsman, D. D. Klebanova, A. A. Grigor'ev, *Theor. Exper. Chem. (Russian)* **1987**, 191.
[38] D. N. Laikov, Yu. A. Ustynyuk, in [35], B. 17.
[39] K. Hafner, H. Diehl, H. U. Süss, *Angew. Chem.* **1976**, *88*, 121; *ibid., Int. Ed. Engl.* **1976**, *15*, 104.
[40] K. Hafner, H. Kaiser, *Org. Synth., Coll. Vol.* 1973, *5*, 1088.
[41] P. Uebelhart, H.-J. Hansen, *Helv. Chim. Acta* **1992**, *75*, 2493; Y. Chen, H.-J. Hansen, *ibid.* **1993**, *76*, 168.
[42] N. Hock, Ph. D. Thesis, Technical University of Darmstadt, 1991.
[43] M. Lutz, A. Linden, K. Abou-Hadeed, H.-J. Hansen, *Helv. Chim. Acta* **1999**, *82*, 372.
[44] 'Vogel's Textbook of Practical Organic Chemistry', 4th edn., Longman Scientific & Technical, Essex 1987, p. 302.
[45] A. C. T. North, D. C. Phillips, F. S. Mathews, *Acta Crystallogr., Sect. A* **1968**, *24*, 351.
[46] J. De Meulenaer, H. Tompa, *Acta Crystallogr.* **1965**, *19*, 1014.
[47] G. M. Sheldrick, SHELXS86. *Acta Crystallogr., Sect. A* **1990**, *46*, 467.
[48] a) E. N. Maslen, A. G. Fox, M. A. O'Keefe, in 'International Tables for Crystallography', Vol. C, Ed. A. J. C. Wilson, Kluwer Academic Publishers, Dordrecht, 1992; Table 6.1.1.1, p. 477; b) D. C. Creagh, W. J. McAuley, *ibid.*, Table 4.2.6.8, p. 219.
[49] R. F. Stewart, E. R. Davidson, W. T. Simpson, *J. Chem. Phys.* **1965**, *42*, 3175.
[50] J. A. Ibers, W. C. Hamilton, *Acta Crystallogr.* **1964**, *17*, 781.
[51] TEXSAN. Single Crystal Structure Analysis Software, Version 5.0. Molecular Structure Corporation, The Woodlands, Texas, 1989.
[52] C. K. Johnson, ORTEPII. Report ORNL-5138, Oak Ridge National Laboratory, Oak Ridge, Tennessee 1976.

Received July 19, 1999